

# Discovery of antimicrobial peptides with notable antibacterial potency by an LLM-based foundation model

Jike Wang<sup>1,2†</sup>, Jianwen Feng<sup>3†</sup>, Yu Kang<sup>1†</sup>, Peichen Pan<sup>1</sup>, Jingxuan Ge<sup>1</sup>, Yan Wang<sup>3</sup>, Mingyang Wang<sup>1</sup>, Zhenxing Wu<sup>1</sup>, Xingcai Zhang<sup>4,5,6</sup>, Jiameng Yu<sup>7</sup>, Xujun Zhang<sup>1</sup>, Tianyue Wang<sup>1</sup>, Lirong Wen<sup>8</sup>, Guangning Yan<sup>9</sup>, Yafeng Deng<sup>2†</sup>, Hui Shi<sup>2</sup>, Chang-Yu Hsieh<sup>1\*</sup>, Zhihui Jiang<sup>3,7,10\*</sup>, Tingjun Hou<sup>1\*</sup>

Large language models (LLMs) have shown remarkable advancements in chemistry and biomedical research, acting as versatile foundation models for various tasks. We introduce AMP-Designer, an LLM-based approach, for swiftly designing antimicrobial peptides (AMPs) with desired properties. Within 11 days, AMP-Designer achieved the de novo design of 18 AMPs with broad-spectrum activity against Gram-negative bacteria. In vitro validation revealed a 94.4% success rate, with two candidates demonstrating exceptional antibacterial efficacy, minimal hemotoxicity, stability in human plasma, and low potential to induce resistance, as evidenced by significant bacterial load reduction in murine lung infection experiments. The entire process, from design to validation, concluded in 48 days. AMP-Designer excels in creating AMPs targeting specific strains despite limited data availability, with a top candidate displaying a minimum inhibitory concentration of 2.0 micrograms per milliliter against *Propionibacterium acnes*. Integrating advanced machine learning techniques, AMP-Designer demonstrates remarkable efficiency, paving the way for innovative solutions to antibiotic resistance.

Copyright © 2025 The Authors, some rights reserved; exclusive licensee American Association for the Advancement of Science. No claim to original U.S. Government Works. Distributed under a Creative Commons Attribution NonCommercial License 4.0 (CC BY-NC).

## INTRODUCTION

Bacterial antimicrobial resistance (AMR) poses a major global threat to human health. It has been estimated that almost 4.95 million deaths were associated with bacterial AMR globally in 2019, including 1.27 million deaths attributable to bacterial AMR (1), which had been predicted to rise to 10 million deaths per year by 2050 (2). Gram-negative bacteria are particularly troubling as they have developed resistance to most commonly used antibiotics. This alarming situation is further exacerbated by the fact that no new class of antibiotics that are effective against Gram-negative bacteria has passed the clinical stage since the introduction of quinolones in 1968 (3).

Typically ranging from 10 to 50 amino acids in length, antimicrobial peptides (AMPs) are naturally produced by various organisms to combat invading microorganisms (4). Because of their remarkable diversity in structures and functions, along with their good efficacy and reduced likelihood of resistance development, AMPs have been considered as potential alternatives to conventional small-molecule antibiotics. However, compared to small-molecule-based antibiotics, many AMPs suffer from serious limitations such as relatively lower

antibacterial activity, uncertain toxicity profiles, and susceptibility to inactivation during production and transportation (5–8), impeding their widespread application. To address these challenges, current research focuses on developing AMP candidates with enhanced activity, reduced toxicity, and increased resistance to hydrolysis. These improvements should make AMPs as contending antibiotics.

In recent years, there has been a growing interest in leveraging computer-aided methods to expedite the design of AMPs (9). Conventional methods for designing AMPs typically involve optimizing existing AMPs or using AMP prediction models (10–18) to exhaustively screen a large-scale peptide space. However, the vast size of the peptide sequence space, estimated to cover approximately  $4.5 \times 10^{41}$  peptides with the sequence length up to 32 residues (19), poses a formidable challenge of discovering new AMPs. Moreover, despite substantial efforts, only about 10 AMPs have been approved by regulatory agencies (20), indicating that the therapeutically relevant AMPs are sparsely distributed across this vast sequence space. Consequently, there is an urgent need to develop novel approaches for more effective AMP design.

With the advancement of deep generative modeling techniques, new AMP design methods have emerged (21, 22), including those based on recurrent neural networks (RNNs) (23–25), generative adversarial networks (GANs) (19, 26–29), and variational autoencoders (VAE) (30–33). Designing AMPs with multiple desired traits, such as high activity and low hemolysis, is a nontrivial task. To generate AMPs with these desired traits, existing approaches rely on the paradigm of supervising learning with few labeled data. As models only learn from experimentally validated and labeled AMPs, this leads to low novelty for generated AMP sequences. One strategy to sample from a wider peptide space and to improve novelty is to train generative models on a broader dataset containing all kinds of natural peptides. But this naive strategy cannot guarantee a high probability of generating AMPs with the desired traits. This dilemma (novelty versus validity) is usually formulated as a problem of multicondition

<sup>1</sup>College of Pharmaceutical Sciences, Zhejiang University, Hangzhou 310058, Zhejiang, China. <sup>2</sup>CarbonSilicon AI Technology Co. Ltd., Hangzhou 310018, Zhejiang, China.

<sup>3</sup>School of Pharmaceutical Sciences, Southern Medical University, Guangzhou 510515, Guangdong, China. <sup>4</sup>John A. Paulson School of Engineering and Applied Sciences, Harvard University, Cambridge, MA 02138, USA. <sup>5</sup>World Tea Organization, Cambridge, MA 02139, USA. <sup>6</sup>Department of Materials Science and Engineering, Stanford University, Stanford, CA 94305, USA. <sup>7</sup>Graduate School, Guangzhou University of Chinese Medicine, Guangzhou 510006, Guangdong, China. <sup>8</sup>School of Pharmaceutical Sciences, Dali University, Dali 671003, Yunnan, China. <sup>9</sup>Department of Pathology, General Hospital of Southern Theatre Command, Guangzhou 510010, China. <sup>10</sup>Department of Pharmacy, General Hospital of Southern Theatre Command, Guangzhou 510010, Guangdong, China.

\*Corresponding author. Email: tingjunhou@zju.edu.cn (T.H.); jandsphy@163.com (Z.J.); kimsieh@zju.edu.cn (C.-Y.H.)

†These authors contributed equally to this work.

‡Present address: Department of Automation, Tsinghua University, Beijing 100084, China.

generations. Conditional GANs (34) and conditional VAEs (35) have emerged as popular solutions to this challenge (19), but their reliance on labeled data for training has been an issue. The process of labeling the dataset using AMP predictors or assuming unlabeled data as negative samples can introduce biases and result in substantial prediction errors during the training stage. Fine-tuning (FT) on small datasets of experimentally labeled AMPs is another feasible approach (36, 37). However, traditional methods of FT large-scale models suffer from high computational costs and the risk of overfitting to small datasets (38–40). Alternatively, a classifier trained on the latent space (32, 41) can identify regions where AMPs with desired traits reside and be combined with rejection sampling to generate the desired sequences with an improved success rate.

The emergence of ChatGPT recently has captured the wildest imagination of the crowd. AMP generation is a specific task of protein language modeling, which has greatly benefited from the development of large language models (LLMs) for natural language processing (NLP). Drawing analogy from NLP and other protein design cases, we have reasons to believe that large-scale sequence generation models can also excel for AMP design. Adapting an LLM for downstream tasks, prompt tuning has gradually replaced traditional FT methods. Compared to FT, prompt tuning offers higher computational efficiency and greater flexibility without having to retrain the model. Moreover, it provides a means to mitigate overfitting to some extent and effectively bridges the gap between pretraining and downstream tasks (39, 42, 43). In the context of conditional generation tasks, achieving a balance between generation diversity and success rate is crucial, making prompt tuning an appropriate approach.

In this work, we proposed AMP-Designer, a comprehensive framework for AMP design that integrates GPT (44), prompt tuning (45), contrastive learning, knowledge distillation, and reinforcement learning (RL), followed by a series of wet-lab analyses for the validation of the designed AMPs (Fig. 1). Our approach involves training an AMP-centric language model as the foundation model, AMP-GPT, on a dataset of peptides extracted from UniProt (46). To facilitate transfer learning on a labeled dataset of AMPs and enable the generation of peptide sequences with desirable traits, we used AMP-Prompt, i.e., contrastive prompt learning while keeping the parameters of AMP-GPT frozen. To further reduce computational costs, we performed model distillation on AMP-Prompt, by compressing it into an RNN composed of three gated recurrent unit (GRU) layers, namely AMP-Distillation. In addition, we constructed the minimum inhibitory concentration (MIC) prediction models, AMP-MIC, based on AMP-GPT for different bacterial species, providing feedback and facilitating subsequent screening with RL.

Using AMP-Designer, we achieved rapid de novo design of highly diverse and potent AMPs against given bacteria species. Selection and synthesis of the top 20 AMP candidates (two peptides failed after three rounds of chemical syntheses) based on the average prediction scores provided by AMP-MIC enabled the discovery of two wet-lab validated exceptional AMPs, KW13 and AI18, within 48 days (Fig. 1A). These two peptides exhibited strong *in vitro* antibacterial activity against a diverse set of Gram-negative bacteria and Gram-positive bacteria. Notably, both newly designed peptides demonstrated low off-target hemolysis toxicity, excellent plasm stability, and strong antibacterial activity against a collection of clinically derived resistant Gram-negative bacteria. KW13 and AI18 at sub-MIC concentration did not induce drug resistance in *Escherichia coli* after 30 generations of culture. Furthermore, they

showed remarkable therapeutic efficacy in a bacterial pneumonia mouse model.

AMP-Designer is a plug-and-play framework. For new design tasks, it only takes around 3 days to complete the design based on the trained foundation model AMP-GPT. Notably, AMP-Designer demonstrates excellent efficacy in designing specific AMPs even in scenarios with severely restricted labeled data, which are frequently encountered in real-world situations. To illustrate this capability, we designed AMPs against *Propionibacterium acnes* (also known as *Cutibacterium acnes*), an anaerobic microorganism with extremely scarce labeled data points (less than 20). Given the impracticality of training an MIC predictor of *P. acnes* for guiding model optimization through RL in this context, we used AMP-Designer to generate five AMP candidates against *P. acnes*, among which three displayed high potency during subsequent experimental evaluations. The successful few-shot AMP design highlights the commendable adeptness of the AMP foundation language model in conjunction with the AMP discovery workflow, in effectively navigating the AMP space.

## RESULTS

### AMP-Designer: The overview

The AMP-Designer workflow is presented in Fig. 1B, depicting the model and training details. Initially, a collection of peptides with lengths less than or equal to 32 was gathered from UniProt (46), resulting in a dataset comprising 630,683 peptides. These peptides were used to conduct unsupervised training of AMP-GPT. Compared to training on small labeled datasets, leveraging a larger and more diverse dataset enables AMP-GPT to learn a more comprehensive representation of the data, a well-established phenomenon for large-scale language and biological models (47–53). Subsequently, the objective is to identify sequences with antimicrobial activity within the peptide space learnt by AMP-Designer. To achieve this, a curated set of 9896 positive samples and 2403 negative samples were retrieved from various AMP databases. Using these labeled samples, contrastive prompt tuning was applied to fine-tune the model, specifically initializing the prompt embedding layer based on the word embedding of AMP-GPT, and the labeled data were used to train this layer while holding the parameters of AMP-GPT fixed. The resulting model obtained through this process is referred to as AMP-Prompt.

While the integration of top-*k* (54, 55) sampling has shown remarkable success rates in generating AMPs (detailed in the “Activity analysis” section, where three AMP predictors were used to assess the generated sequences), it is important to acknowledge that AMP-Prompt is prompt-tuned on a binary-class dataset of AMPs. Therefore, the model is limited to binary-class generation, lacking the ability to impose constraints on generating other desired properties. In a real-world scenario, a therapeutic AMP has to satisfy multiple requirements, such as manifesting higher activity or targeting specific bacteria. Therefore, further optimization is needed on top of AMP-Prompt to meet these additional criteria. ChatGPT has achieved tremendous success by leveraging the technique of RL from human feedback, where the core idea is to use expert knowledge to score the generated sequences and provide feedback for the RL agent. For AMP design, scoring the generated sequences based on human expertise is challenging (refer to Methods for more algorithm details).

Numerous properties influence the activity of AMPs. For instance, AMPs often exhibit a certain degree of hydrophobicity and

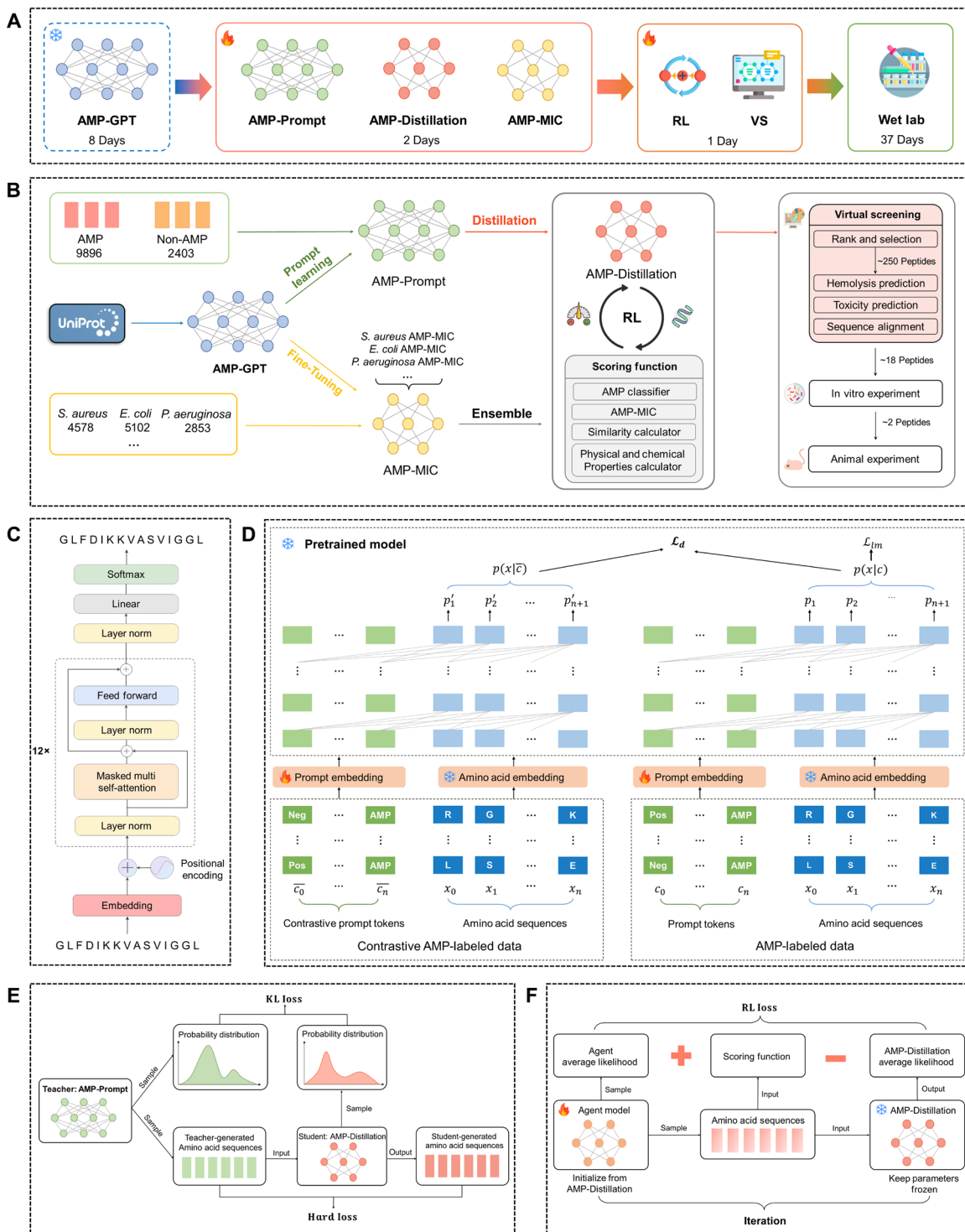


**Fig. 1. The overview of AMP-Designer.** (A) The timeline for antimicrobial peptide (AMP) screening using AMP-Designer, followed by the in vitro and in vivo validations. (B) Workflow of AMP-Designer. VS, virtual screening. (C) Architecture of AMP-GPT. (D) Contrastive prompt fine-tuning (FT) process. (E) Model distillation process. (F) Reinforcement learning (RL) optimization process.

hydrophilicity, contributing to their interactions with bacterial membranes. The balance between hydrophobic and hydrophilic characteristics can affect the targeting efficiency and solubilization capacity of AMPs. In addition, the presence of a higher positive charge affects the charged nature of AMPs, influencing their interactions with bacterial membranes. Cationic AMPs, in particular, demonstrate an inclination to interact with anionic molecules within bacterial membranes, thereby eliciting perturbation of the cellular membrane. Furthermore, the prevalence of  $\alpha$ -helical secondary structures is noteworthy. Many AMPs adopt  $\alpha$ -helical conformations during their interactions with membranes. This particular structural motif facilitates the insertion of AMPs into the lipid bilayer of cellular membranes, thereby inducing membrane disruption. Therefore, building upon AMP-GPT, we trained the AMP-MIC predictors for different bacteria, considering properties such as electric charge, to provide feedback for RL (refer to the “Design high-activity against Gram-negative bacteria peptides” section for more details).

However, performing RL optimization directly on AMP-Prompt, which is based on GPT, requires substantial computational resources. To address this issue, we used knowledge distillation, leading to the development of a more compact model termed AMP-Distillation that maintains a comparable generative capability to that of AMP-GPT. Subsequently, RL was applied to optimize AMP-Distillation, facilitating the identification and selection of the most optimal candidate AMPs suitable for the subsequent syntheses.

### Analysis of physical and chemical properties

We randomly selected 2000 peptide sequences from both the generative model and real AMPs for analysis. We used an analysis tool

from modlAMP (56) to visualize the distribution of amino acid frequencies, total charge, Eisenberg hydrophobicity, Eisenberg hydrophobic moment (57), and sequence length of these peptides. These fundamental attributes serve to facilitate our analysis of the model’s learning dynamics, encompassing an assessment of whether the foundational model has effectively captured the distribution across the entirety of the small peptide space. Furthermore, this enables an evaluation of whether the subsequent FT of the model has effectively assimilated the distribution inherent to the real AMPs.

As shown in Fig. 2, the distributions of the physicochemical properties of the peptides generated by AMP-GPT are similar to those of the UniProt training dataset. This observation demonstrates that AMP-GPT has effectively learned the physicochemical characteristics of peptides in the UniProt training dataset. After contrastive prompt learning, we observed a notable shift in the distribution of various physicochemical properties of the generated peptide sequences. The properties of these newly generated peptides were closer to those of the real AMPs, indicating the effectiveness of our prompt tuning. We further used top- $k$  sampling to generate peptides after prompt learning and found that, compared to traditional temperature-based sampling, top- $k$  sampling resulted in a distribution of peptides with higher global charge and modified physicochemical properties, such as Eisenberg hydrophobicity and hydrophobic moment, which were more similar to those of the real AMPs. As most reported AMPs are cationic and amphiphilic in nature and have properties that are thought to be crucial for insertion into and disruption of the bacterial outer membrane which is the main cause of resistance and inactivity of many antibiotics (5) Last, the distillation model produced peptide

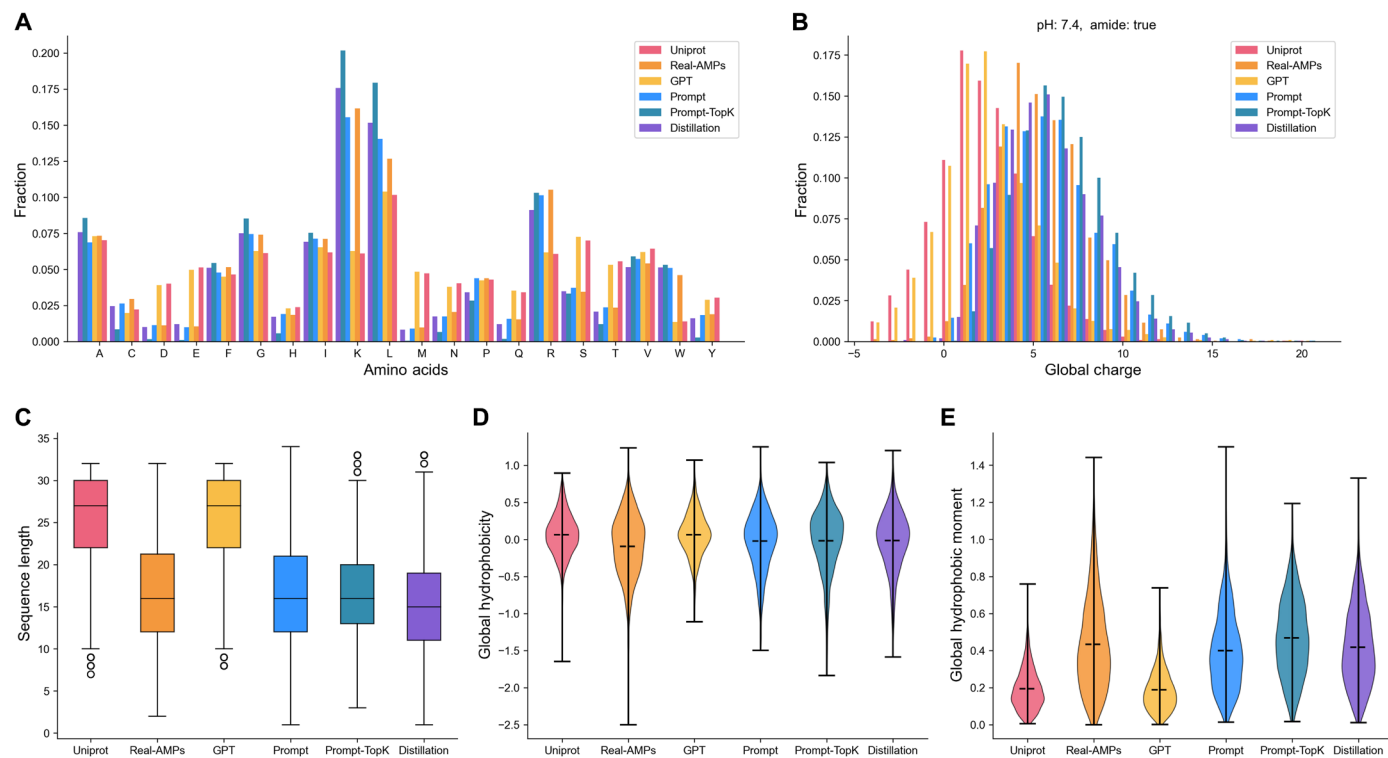


**Fig. 2. Comparison of physicochemical properties.** UniProt (red), real antimicrobial peptides (AMPs) (orange), AMP-GPT (yellow), AMP-Prompt (blue), AMP-Prompt-TopK (green), and AMP-Distillation (purple) distributions of the physical and chemical properties of peptides: (A) amino acid, (B) global charge, (C) sequence length, (D) Eisenberg hydrophobicity, and (E) Eisenberg hydrophobic moment.

sequences with physicochemical property distributions that were highly similar to those generated by the teacher model, demonstrating that it successfully learned the probability distribution of the teacher model.

### Activity analysis

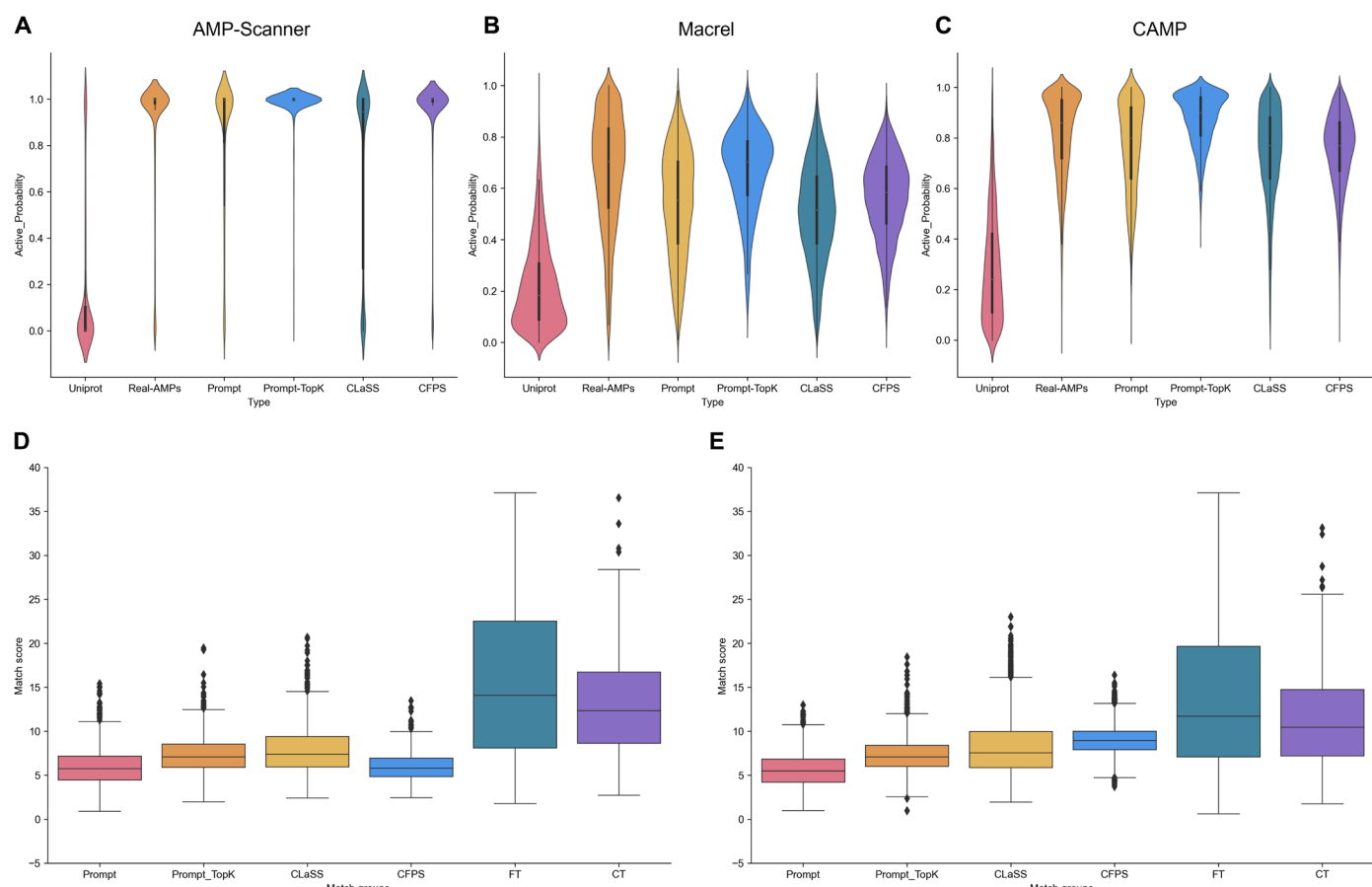
To evaluate the generated peptides, we used three different AMP classifiers: The predictor based on the collection of anti-microbial peptides (CAMP) (58), AMP Scanner (59), and Macrel (60), to assess their potential for bioactivity. We introduced the state-of-the-art (SOTA) methods, CLaSS (32) and cell-free protein synthesis (CFPS) (61), as baselines for comparison. Following the recommendation by AMP Scanner that the predictions for sequences with less than 10 amino acids should be interpreted with caution, we selected multipeptide sequences with a length of 10 or higher for our evaluation.

Figure 3 (A to C) illustrates a notable enhancement in the performance of the Prompt-based model across all three predictors. In particular, the peptides generated by Prompt-TopK exhibit a distribution of bioactivity that closely mirrors that of real AMPs. In general, a predictor assigns a sequence as an active AMP when the output is 0.5 or higher. It is evident that the performance of the candidate AMPs generated by various models aligns consistently with the expectations across all three predictors. Notably, AMP-GPT demonstrates a strong ability to learn from the peptide data in UniProt,

as the generated peptides exhibit an activity probability distribution to that of the peptide sequences from UniProt, consistently below 0.5 across all three predictors. However, after postprompt tuning, the candidate AMPs generated by the model display activity probabilities comparable to those of real AMPs. In particular, the performance of the Prompt-TopK variant even surpasses that of real AMPs, with probabilities centered around 1. Furthermore, our method consistently exhibits significantly higher probabilities of being predicted as active by all three predictors compared to CLaSS and CFPS.

Hence, we further calculated the percentage of the peptide sequences identified as AMPs by all three predictors simultaneously (with predicted values of 0.5 or higher). As illustrated in Table 1, the percentages are 50.7% for CLaSS and 57.2% for CFPS. In contrast, our approach achieves a substantially higher percentage of 83.4%, outperforming CFPS by 26.2%, marking a considerable advancement. Our findings reveal that the predicted activity probability for peptides generated by Prompt-TopK exceeds that of real AMPs.

Furthermore, the distillation model maintained nearly identical performance to the AMP-Prompt as shown in table S1. Drawing upon the analysis of the physicochemical properties presented in the preceding section, it can be deduced that the student model, denoted as AMP-Distillation, has proficiently acquired the probability distribution inherent to the teacher model, AMP-Prompt.



**Fig. 3. Activity probability and match scores distribution.** (A to C) Activity probability distribution predicted by three antimicrobial peptide (AMP) predictors. (D and E) Match scores distribution. Distributions of the match scores between (D) real AMPs and (E) generated internal sequences.

## Diversity and novelty analysis

We further conducted an analysis on the validity, uniqueness, and novelty of the peptides generated by our proposed method, as well as two baseline methods: conditional token (CT) and full model FT. Specifically, the condition token method is retrained on labeled data, and a property label is added to the model during training, which is used as the input during generation to autoregressively generate the entire peptide sequence. The traditional FT directly fine-tuned the AMP-GPT model using the real AMP dataset. For detailed information, please refer to the “CT and FT models” section in Methods. Validity indicates whether the generated sequence is valid, uniqueness denotes the percentage of unique peptides generated, and novelty represents the percentage of peptides that are different from the real AMPs.

In the analysis, it is evident that the CT produces invalid sequences, such as “[mask]” indicating a suboptimal learning of the distribution of amino acid sequences in AMPs. Furthermore, the comparison presented in Table 2 reveals that the uniqueness and novelty metrics of the sequences generated by the FT are inferior to those generated by the prompt-based method. This observation suggests a higher degree of overfitting in the FT, as it generates sequences that exhibit repetition either within themselves or to the real AMPs.

This can be attributed to the fact that the CT and FT methods retrain the entire model on the real AMPs, which can easily cause overfitting. Conversely, our prompt-based approach freezes the pre-trained model parameters and only trains the parameters of the embedding layer on the real AMPs, so they perform better than the CT and FT in terms of diversity and novelty, while maintaining a high activity likelihood for the generated peptides.

To further explore the diversity of the generated peptides, we used the pairwise2.align.globalxx method from biopython (62) for sequence alignment and calculated the match scores of the

generated sequences. The approach involves pairwise comparisons of the generated AMP sequences with the corresponding sequences (real AMPs or internal sequences) to determine the highest match score. Figure 3D illustrates the match scores between the generated sequences and the real AMPs. Notably, our approach illustrates a lower resemblance to the real AMPs compared to the baselines. In addition, we compared the internal similarity among the generated AMP sequences across various models (Fig. 3E), revealing that our method demonstrates overall lower internal similarity relative to the other models. The findings suggest that our approach not only enhances the probability of activity but also maintains a higher degree of diversity, leading to the generation of more novel peptide sequences.

## Design high-activity against Gram-negative bacteria peptides

While the outlined approaches yield bioactive candidate AMPs, quantifiable control over the inherent properties of the generated candidates, such as their degree of activity and net charge, remains elusive. Therefore, to obtain AMP with higher activity and other desired properties, RL was used for further optimization.

In the course of RL optimization, the reward function incorporates five distinct components, namely classification probability (CP), MIC against three bacterial strains, sequence length (SL), memory similarity (MS), and charge. Detailed information regarding these components can be found in table S4. The classification probability is the prediction result calculated by Macrel, which is a SOTA AMP predictor (63). Meanwhile, the MIC was predicted by three AMP-MIC models which were trained using the MIC data of three different bacteria (*Staphylococcus aureus*, *Pseudomonas aeruginosa*, and *E. coli*). The accuracy of the AMP-MIC predictor is compared to that of the RNN model proposed by Huang *et al.* (64) and the GPT-based model trained from scratch, as shown in table S5. Our experimental results demonstrate that the AMP-MIC achieves a higher accuracy than the other two models. To increase the diversity of the generated sequences, we did not directly use the continuous numerical values of the classification probably and MIC as the rewards in RL.

To clarify the contributions of RL, we conducted a comprehensive analysis by sampling molecules at each step during the RL tuning process. This allowed us to explore the relationship between the number of RL steps and the average scores achieved for generated AMPs. By examining the variations in average scores at different RL steps, we gained insights into the impact of RL on the generation of AMPs and the corresponding improvements in their quality.

As shown in fig. S3 (A to C), the *x* axis represents the RL steps, while the *y* axis represents the respective average scores (AMP

**Table 1. Percentage of the peptides identified as antimicrobial peptides (AMPs) by all three predictors simultaneously.**

Type	Percentage
UniProt	4.58%
Prompt	61.8%
Prompt-TopK	83.4%
CLaSS	50.7%
CFPS	57.2%
Real-AMPs	81.4%

**Table 2. Validity, uniqueness, and novelty of five models.**

Model	Validity	Uniqueness	Novelty
CT	97.9%	91.8%	84.4%
FT	100%	88.3%	73.1%
AMP-Prompt	100%	99.9%	99.6%
AMP-Prompt-TopK	100%	100%	99.9%
AMP-Distillation	100%	99.8%	99.7%

predicted score, *E. coli* predicted MIC, and *P. aeruginosa* predicted MIC). It is evident that the average scores (activity probabilities) of the AMP predictor increase from 0.5 to more than 0.7 as the number of steps in RL increases. Furthermore, the predicted MIC against *E. coli* and *P. aeruginosa* decreases from more than 500 to below 5.

Subsequently, we visualized the distributions of three properties for the generated AMPs at 10, 30, and 50 steps. As depicted in fig. S3D, there is a clear improvement in the average scores of the AMP predictor from the 10th step to the 50th step. To better visualize the distributions of predicted activity against *E. coli* and *P. aeruginosa*, we capped values above 20 at 20. As shown in fig. S3 (E and F), the distribution of activity becomes increasingly concentrated from the 10th step to the 50th step, with most values falling below 5.

Moreover, we used a memory queue to store the top 256 AMPs with the highest scores to increase the diversity of the generated sequences. During the RL process, 128 amino acid sequences were sampled to evaluate the current state, and those with higher scores were added to the memory queue, replacing those with lower scores. Memory similarity was calculated by comparing the sampled peptides with the peptides in the memory queue using the biopython's pairwise2.align.globalxx method (62) and then divided by the length of the sequence. The final reward, which incorporates all the aforementioned factors, is given in Eq. 18. We sorted the scores of the generated peptide sequences and retained the top 250 peptides produced by the RL agent for further screening. Next, we calculated the AMP classification probabilities for CAMP, AMP Scanner, and Macrel, the  $\alpha$ -helical score was calculated by biopython, the hemolysis score was predicted by HemoPI (65), and the toxicity score was predicted by ToxinPred (66, 67). On the basis of the aforementioned screening procedure, we retained the predicted AMP sequences that exhibited an  $\alpha$ -helical structure with a hemolytic probability below 0.6 and were predicted to be nontoxic. Subsequently, we sorted these sequences based on their predicted scores for *P. aeruginosa* and *E. coli*. After excluding all noncompliant candidates, we identified the top 20 candidates based on the average prediction scores given by AMP-MIC testing against two Gram-negative bacteria: *P. aeruginosa* and *E. coli*.

### In vitro activities of the leading AMPs against members of ESKAPE

The top 20 predicted AMPs were chosen for chemical synthesis and verification. Two peptides failed to synthesize even after three rounds of attempts. We then tested in vitro antibacterial activities of the 18 candidates. First, we determined the MIC values of those AMPs against six standard strains of all members of ESKAPE [*Enterococcus faecalis* American Type Culture Collection (ATCC) 29212, *S. aureus* ATCC 29213, *Klebsiella pneumoniae* ATCC 700603, *Acinetobacter baumannii* ATCC 19606, *P. aeruginosa* ATCC 27853, and *E. coli* ATCC 25922]. As shown in Table 3, 17 of 18 candidates exert notable antibacterial activity against at least one strain. In general, the majority of AMPs are more effective against Gram-negative bacteria than Gram-positive bacteria, which is to some extent aligned with our specific design of AMPs targeting Gram-negative bacteria. Moreover, the remarkable activity of these AMPs, initially designed for *P. aeruginosa* and *E. coli*, extends to *K. pneumoniae* and *A. baumannii* as well, suggesting that these AMPs may have a general bactericidal mechanism against Gram-negative bacteria. AI18, KW13, KW20, RV15, and GI16 exhibited the highest antibacterial activity against both Gram-negative bacteria (MICs range from 4 to 16  $\mu\text{g}/\text{ml}$ ) and Gram-positive bacteria

(MICs range from 8 to 32  $\mu\text{g}/\text{ml}$ ), suggesting more excellent broad-spectrum activities across all tested ESKAPE strains. Consequently, we further evaluated the activities of AI18, KW13, KW20, RV15, and GI16 against six strains of clinically resistant Gram-negative bacteria [pan-drug resistant (PDR) *K. pneumoniae* 418015, extensive-drug resistant (XDR) *K. pneumoniae* 325016, multidrug resistant (MDR) *K. pneumoniae* 327004, MDR *E. coli* 103231, MDR *P. aeruginosa* 304238, and MDR *A. baumannii* 316039], and the results are shown in Table 4. All five AMPs showed notable activities against five strains of superbugs, with MICs ranging from 4 to 16  $\mu\text{g}/\text{ml}$ ; however, it is worth noting that KW13 and AI18 demonstrated only moderate activities against PDR *K. pneumoniae* 418015, a colistin (COL)-resistant strain (table S6).

A thorough analysis was performed to compare the MIC values and sequence diversity of the AMPs designed by artificial intelligence (AI) in recent studies (32, 64). The sequence diversity was assessed between the generated AMPs and biological patent sequences using the patseqfinder tool available on LENS.ORG (68). The outstanding performance of our designed peptides across various aspects is evident from the results presented in table S7.

Off-target toxicity, especially hemolysis, is a major concern for cationic AMPs. We evaluated hemolysis of human erythrocytes in the presence of AI18, KW13, KW20, RV15, or GI16. As displayed in Fig. 4A, KW13 and AI18 demonstrated negligible hemolysis effects. We further determined the 50% hemolytic concentration (HC50, 50% hemolysis) of these two AMPs. Their HC50 values were both higher than 1000  $\mu\text{g}/\text{ml}$ , which quantitatively demonstrated their excellent hemocompatibilities (fig. S4).

To more comprehensively assess the bactericidal effects of KW13 and AI18, we conducted time-kill studies against *E. coli* ATCC 25922. As shown in Fig. 4B, KW13 and AI18 can significantly reduce viable counts after 2-hour incubation, and the bactericidal effect lasted at least for 24 hours, while the last resort antibiotic COL only exerts bactericidal effect for about 8 hours.

The propensity to induce bacterial resistance is recognized as a challenging feat for AMPs, given their mode of action which primarily targets bacterial membranes rather than engaging a specific receptor (69). We assessed possible antibacterial resistance by culturing *E. coli* ATCC 25922 with the sub-MIC level of KW13 and AI18, using the classic small-molecule antibiotic norfloxacin for comparison. As shown in Fig. 4C, *E. coli* could not develop obvious resistance against KW13 and AI18 after 30 generations, as is the case against COL. In contrast, the bacteria started to develop resistance to norfloxacin after 17 generations, with a 128-fold reduced susceptibility after 30 generations.

As the plasma stability of an AMP is an important factor in its ability to exert in vivo efficacy, we first evaluated the proteolytic stability of KW13 and AI18 before evaluating their in vivo antibacterial efficacy. As shown in Fig. 4D, KW13 and AI18 degraded slowly in human plasma in 4 hours, indicating that KW13 and AI18 have great plasma stability.

We then focused on elucidating the membrane disruption effect of KW13, which showed the highest activity in vitro against *E. coli*. The common mechanism of action of AMP is bacterial lysis by forming pores on bacteria membranes (70). We used transmission electron microscopy (TEM) to observe the potential morphological changes of membrane in *E. coli* ATCC 25922 cells upon KW13 treatment (MIC = 4  $\mu\text{g}/\text{ml}$ , treated with 1 $\times$  and 10 $\times$  MIC for 5 hours). Figure 4E demonstrated that the cell content leaked out, and the

**Table 3.** In vitro antibacterial activities of top 18 AMPs against six standard ESKAPE strains.

AMPs	MIC <sup>*</sup> (μg/ml)					
	ATCC 29212 <sup>†</sup>	ATCC 29213 <sup>‡</sup>	ATCC 700603 <sup>§</sup>	ATCC 19606 <sup>¶</sup>	ATCC 27853 <sup>#</sup>	ATCC 25922 <sup>**</sup>
RR13	128	64	64	32	32	16
AI18	32	32	16	8	8	8
KW20	16	16	16	16	8	4
KW13	16	8	8	8	4	4
VK18	64	16	16	8	16	16
SK18	16	8	32	8	16	8
RV15	8	8	16	8	16	8
IR20	32	32	32	16	64	32
RK17	64	32	32	8	16	32
LW14	16	16	32	16	64	16
GI16	32	8	16	8	16	16
RR16	256	64	16	16	4	8
YK19	16	16	64	32	32	32
AK15	64	8	16	16	8	8
KK12	>256	>256	>256	>256	>256	>256
KWI18	64	32	64	16	64	32
LF19	16	8	32	8	16	16
AV20	16	8	16	8	32	8

\*Minimal inhibitory concentration.    †*E. faecalis*.    ‡*S. aureus*.    §*K. pneumoniae*.    ¶*A. baumannii*.    #*P. aeruginosa*.    \*\**E. coli*.

**Table 4.** In vitro antibacterial activities of four selected AMPs against six resistant clinically Gram-negative strains.

ID	MIC (μg/ml)					
	PDR <i>K. pneumoniae</i> 418015	XDR <i>K. pneumoniae</i> 325016	MDR <i>K. pneumoniae</i> 327004	MDR <i>E. coli</i> 103231	MDR <i>P. aeruginosa</i> 304238	MDR <i>A. baumannii</i> 316039
AI18	32	8	16	4	16	8
RV15	16	16	16	8	16	8
KW13	32	8	16	8	8	4
KW20	16	8	16	4	8	8
GI16	16	16	16	4	32	4

cells lysed at 1× and 10× MIC in a dose-dependent manner, suggesting that the integrity of the bacteria cell membrane decreased.

Together, the in vitro results indicate that KW13 and AI18 passed a preliminary safety profiling and hold therapeutic potential for treating Gram-negative bacteria. Therefore, we conducted further in vivo evaluation.

### In vivo activities of KW13 and AI18 against bacterial pneumonia in a mouse model

We then tested the therapeutic efficacy of KW13 and AI18 by constructing an XDR *K. pneumoniae* 325016 infected pneumonia mouse model. Hospital-acquired pneumonia infected by carbapenem-resistant *K. pneumoniae* is a major clinical concern, which is difficult to be treated and therefore is associated with high mortality (71). AMP has been recognized as a promising antibiotic alternative to treat lung infections. The experimental setup is shown in Fig. 5A. The

bacterial pneumonia model was constructed by suppressing mouse immunity with cyclophosphamide, followed by intratracheal administration of *K. pneumoniae* 325016. Two doses of AMPs were given, and the lungs were obtained after treatment to count the bacteria load. As shown in Fig. 5B, two AMP-treated groups presented reductions of ~99% in bacteria load, which was significantly lower than that in the blank control phosphate-buffered saline (PBS) group, and their therapeutic effects were comparable to that of the positive control AMP indolicidin (72, 73). Tissue histological analysis showed that the lungs treated with KW13, AI18, and indolicidin remained healthy and had clear alveoli morphology, while the PBS group showed severe tissue damage due to the bacterial infection (Fig. 5C). The above results demonstrate that KW13 and AI18 exert promising in vivo antibacterial activities against resistant *K. pneumoniae*-infected pneumonia without any obvious adverse effects on the host and deserve further investigations.

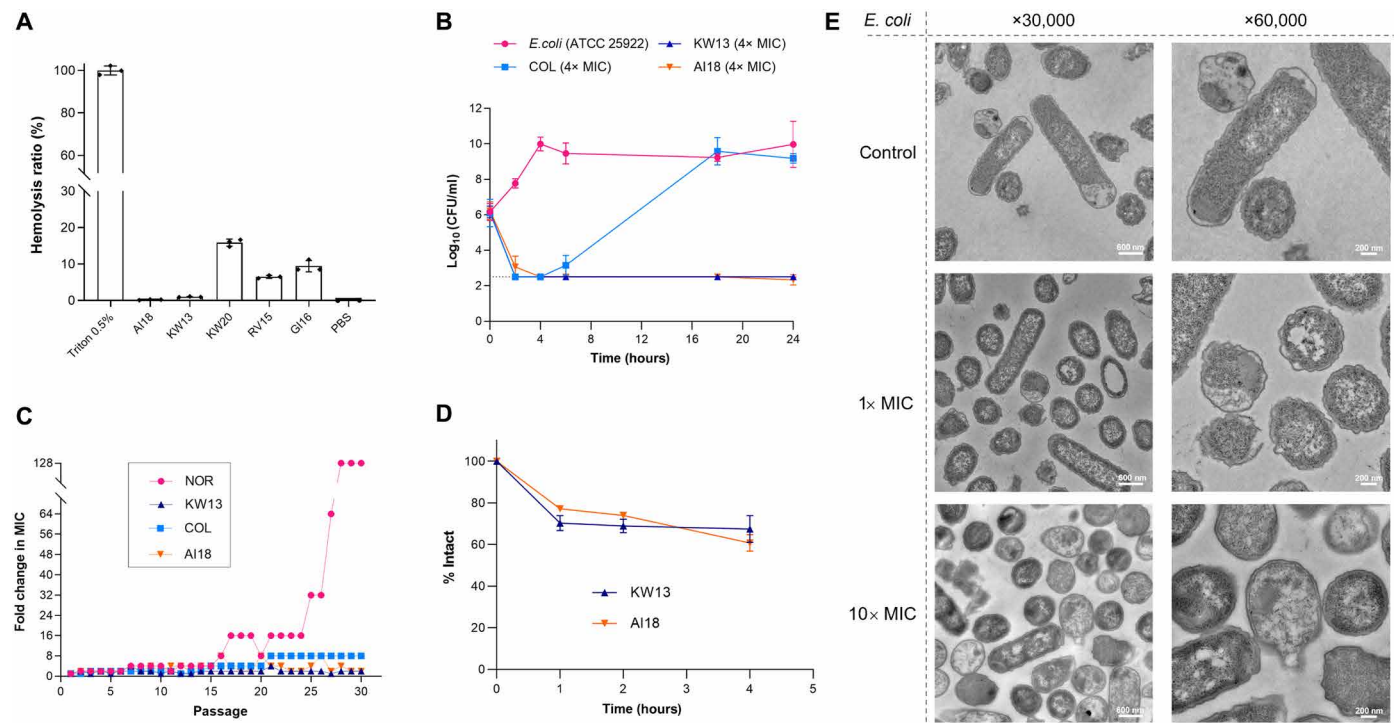


**Fig. 4. Biological properties of the selected antimicrobial peptides (AMPs) in vitro.** (A) Hemolytic activity of KW13, AI18, KW20, RV15, and GI16 at a concentration of 100  $\mu$ g/ml ( $n = 3$  biologically independent replicates, mean  $\pm$  SD). (B) Time-kill curve of KW13 and AI18, with colistin (COL) as positive control ( $n = 3$  biologically independent replicates, mean  $\pm$  SD). (C) Resistance induction studies of *E. coli* ATCC 25922 when cultured in the presence of sub-MIC (1/2x) levels of KW13 and AI18, with norfloxacin (NOR) and COL as positive controls. (D) Human plasma stability testing of KW13 and AI18 by high-performance liquid chromatography (HPLC). Data are shown as mean  $\pm$  SD ( $n = 3$  biologically independent replicates). (E) TEM images of *E. coli* cells treated with KW13 and PBS (control) at  $\times 30,000$  magnification (scale bars, 600 nm) and  $\times 60,000$  magnification (scale bars, 200 nm).

### Few-shot AMP design against *P. acnes*

Acne vulgaris is a chronic skin disorder, which affected more than 630 million people globally, thus being ranked as the eighth most common disease in the world (74). Colonization of anaerobic Gram-positive bacterium *P. acnes* in the pilosebaceous follicles of human skin is closely related to the severity of acne vulgaris (75). Conventional small-molecule antibiotics were commonly used topically or systemically based on the severity of the acne lesion. However, resistance to these antibiotics has been increasing reported (76, 77).

The challenge in this task stems from the scarcity of labeled data pertaining to *P. acnes*. Upon analysis of the entire FT dataset, a total of 47 AMPs is identified with labels indicating explicit activity against *P. acnes*. Among these peptides, 17 have C-terminal amidation and exhibit a length equal to or less than 32 amino acids. Our analysis convincingly revealed a positive correlation between the MIC values against *P. acnes* and the antimicrobial activity against *S. aureus*, *Staphylococcus epidermidis*, and *P. aeruginosa*. In light of this correlation, we used three predictors of antimicrobial activity against *S. aureus*, *S. epidermidis*, and *P. aeruginosa* as the proxy for gauging the potency against *P. acnes*. The overall process closely resembled the one used in the “Design high-activity against Gram-negative bacteria peptides” section. Ultimately, we selected five candidate AMPs for subsequent in vitro experimental validation.

As shown in Table 5, three of the five designed AMPs showed potent activities against *P. acnes*, with MICs ranging from 2 to 8  $\mu$ g/ml, which are the lowest compared to those against Gram-positive

bacteria *S. aureus* and Gram-negative bacteria *E. coli*. The results indicate the specificity of these three AMPs against *P. acnes*, aligning perfectly with our intended design goal for a selectively targeted AMP. Among the three candidates, FI19 displayed the highest efficacy against *P. acnes* with an impressive MIC value of 2.0  $\mu$ g/ml. Property-activity correlation analysis demonstrated that higher hydrophobicity combined with lower net charge likely contributes to enhanced antimicrobial activity. As potent, narrow-spectrum AMPs specifically targeting *P. acnes*, further evaluation and modification of FI19, IF20, and RW20 have great potential in transforming them into highly promising anti-acne antibiotics for systemic use.

### DISCUSSION

Peptide design poses a highly challenging task, and unlike small molecules, peptides are composed of amino acid sequences, and their structures exhibit high flexibility, making expert-based design a daunting process. In recent years, with the advancement of AI, an increasing number of AI-based approaches have been used for drug or material design. Given the similarities between the characteristics of peptides and natural language, leveraging the powerful capabilities demonstrated by recent advancements in GPT, it is believed that using similar language models can expedite the discovery of peptides.

In this study, we present an AMP-centric foundation language model and innovative framework for AMP design, denoted as AMP-Designer. This framework includes the development of the first large-

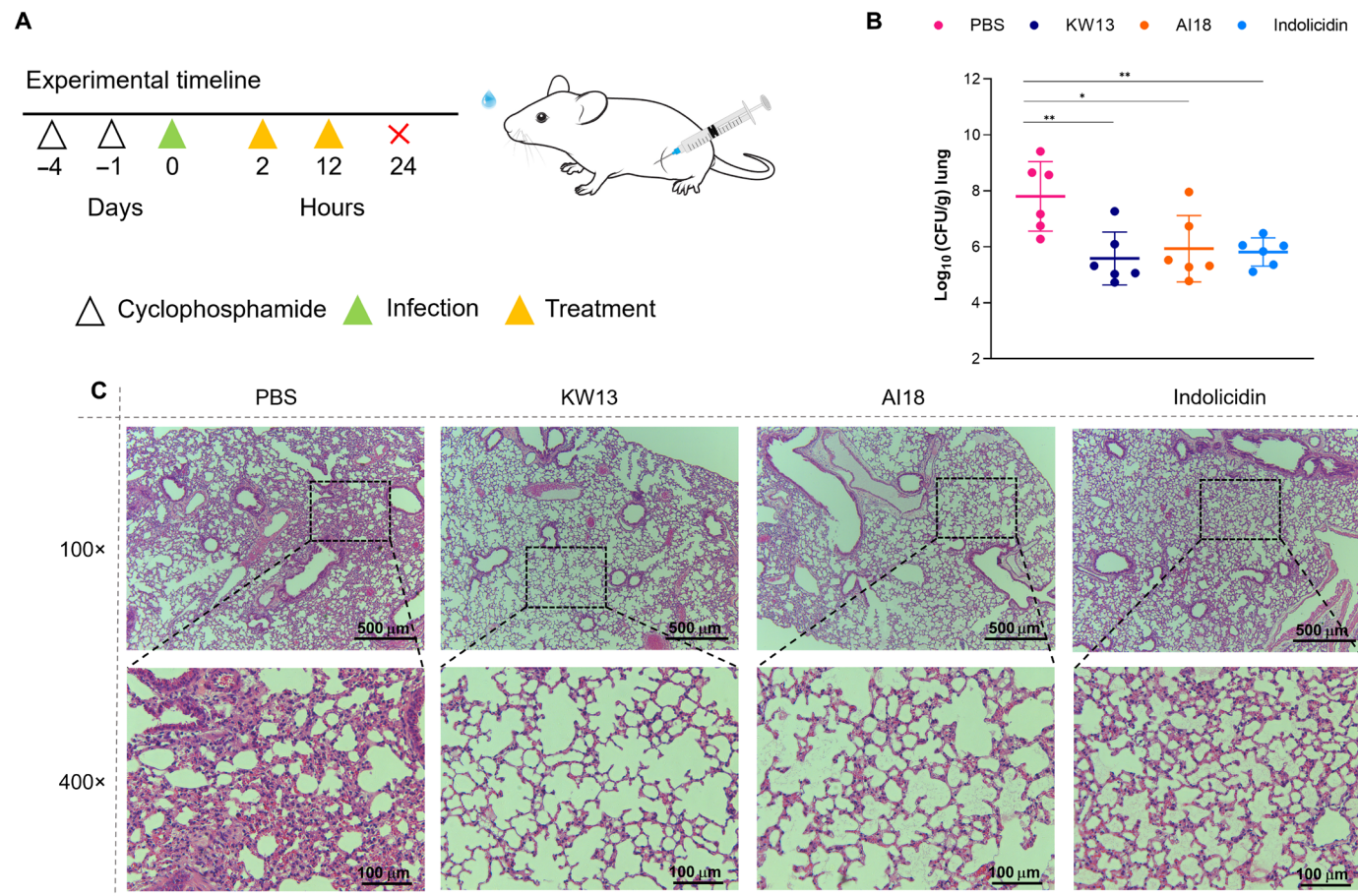


**Fig. 5. In vivo efficacy of KW13 and AI18 in treating mouse pneumonia.** (A) Mouse infection model construction procedures. Mice were injected with cyclophosphamide intraperitoneally twice, followed by the tracheal instillation of XDR *K. pneumoniae* 325016 to establish the pneumonia model. The antimicrobial peptides (AMPs) (10 mg/kg) were injected intraperitoneally twice, and the mice were killed 24 hours after infection. (B) Bacteria load in the lungs of infected mice after treatment with PBS, KW13, AI18, and indolicidin ( $n = 6$  biologically independent replicates, mean  $\pm$  SD). Statistical analysis was performed using one-way analysis of variance (ANOVA). \* $P < 0.05$  and \*\* $P < 0.01$ . (C) Histological images of the lung tissue sections. First row: An overview of the lung tissues after hematoxylin and eosin (H&E) staining (scale bars, 500  $\mu\text{m}$ ). Second row: Detailed histological images in the regions of black boxes (scale bars, 100  $\mu\text{m}$ ). Experiments were performed in duplicates with similar results, and one representative figure is shown.

**Table 5. In vitro antibacterial activities of five antimicrobial peptides (AMPs) against *P. acnes*, *S. aureus*, and *E. coli***

AMPs	MIC ( $\mu\text{g/ml}$ )			
	<i>P. acnes</i> ATCC 6919	<i>P. acnes</i> ATCC 11827	<i>S. aureus</i> ATCC 29213	<i>E. coli</i> ATCC 25922
FI19	2	4	128	64
IF20	4	8	64	64
RW20	64	8	128	64
RW12	32	64	64	64
KW18	64	16	>256	>256

scale pretrained generative model for AMPs, known as AMP-GPT. By incorporating prompt tuning, knowledge distillation, and RL, we notably enhanced the efficiency of AMP generation. In particular, the integration of prompt tuning resulted in an impressive activity prediction rate of 83.4% for AMPs using three SOTA AMP classification predictors, surpassing the proportion observed for real AMPs (81.4%),

while maintaining higher sequence diversity. To further optimize the model for improved AMP activity, we used RL based on multiple properties. In addition, knowledge distillation was applied to reduce computational costs. To validate the performance of AMP-Designer, we specifically focused on designing AMPs against Gram-negative bacteria. Subsequently, 18 peptides were selected for experimental validation.

The *in vitro* experiments confirmed the broad-spectrum effectiveness of the chosen AMPs, of which the top five most active showed potent antibacterial activities against a wide range of clinically relevant Gram-negative pathogens. KW13 and AI18, as two leading AMPs, exhibited therapeutic outcomes comparable to indolicidin in bacterial pneumonia mouse models, with little hemolysis toxicity and a low tendency to induce drug resistance. These results highlight the potential of our AMP-Designer to tackle the pressing issue of the escalating AMR on a global scale and the dwindling antibiotic discovery pipeline. KW13 and AI18 can serve as starting points for structure optimization via peptide cyclization, stapling, or fatty acid modification to support further potency increases and plasma stability enhancement. In addition, to broaden the application of the two AMPs, research on their combination with antibiotics is also necessary.

Furthermore, we devised a few-shot design task targeting *P. acnes*. Leveraging the observed correlation between the AMPs against *P. acnes* and *S. aureus*, we effectively engineered AMPs with exceptional *in vitro* activity against *P. acnes*. While the FT dataset encompasses approximately 20 instances bearing experimental labels specific to *P. acnes*, the overall corpus of authentic real AMP dataset comprises nearly 10,000 distinct AMPs. It is noteworthy that AMP-Designer does not explicitly focus on assimilating the information from these *P. acnes* targeting AMPs. Moreover, this limited subset is inadequate to adequately train an MIC predictor specialized for *P. acnes*, thereby impeding the capacity to optimize for the antimicrobial activity against *P. acnes* in the RL process. Nonetheless, the framework manages to generate remarkably potent AMPs effective against *P. acnes*. This attests to the efficacy of the proposed AMP design workflow based on the peptide foundation model, which has adeptly captured the spatial distribution of diverse AMPs. This capability remains salient even in scenarios where pertinent labeled data are scarce, exemplifying its ability to probabilistically generate highly active AMPs.

Looking ahead, we see an increasing role for cross-modalities of research comprising closely connected, mutually reinforcing experimentation and deep learning. Human-directed experimental trial-error-optimize search strategies of the huge peptide sequence space can frequently lead to highly inefficient resource deployment. Integrating deep learning with targeted wet experiment to guide efficient experimentation and provide new data to improve algorithm performance creates a mutually beneficial cycle that saves labor, money, and time to greatly accelerate AMP discovery and design.

Furthermore, we observed notable potential in generating multiplexed peptide activity through the integration of LLM with the optimization paradigm. The workflow described in this work is generic and extensible, based on the AMP pretraining model AMP-GPT, thereby enabling its seamless integration into various downstream peptide design tasks. The project, encompassing *in silico*, *in vitro*, and *in vivo* aspects, spanned a total of 48 days, in which the computational phase took 11 days. Notably, leveraging the existing AMP-GPT foundation model is expected to further shorten this duration, enabling researchers to accomplish specific peptide generation tasks within a timeframe of 3 days. This permitting them to be straightforwardly translated to the generation of peptides with diverse functions, including immunomodulation, cellular transportation, signaling, and metabolism process.

## METHODS

### AMP-GPT

AMP-GPT is built on the basis of GPT2 small, consisting of 12 layers of Transformer (78) decoder and 8 attention heads. AMP-GPT outputs the token of each amino acid in the peptide in an autoregressive manner. The next generated token is determined by the previously generated character sequence, and masking is used to prevent information leakage from the unencoded characters in the sequence. The multihead self-attention layer is the core of the model, composed of several scaled dot-product attention functions, which enables the model to sequentially capture key information. The attention mechanism is shown in Eq. 1

$$\text{Attention}(Q, K, V) = \text{softmax}\left(\frac{QK^T}{\sqrt{d_k}}\right)V \quad (1)$$

where  $Q$ ,  $K$ , and  $V$  represent the query, key, and value matrices, respectively, and  $d_k$  is the dimension of  $K$ . Since the attention layer can process the entire sequence at the same time, additional positional encoding should be added to each token to ensure the model is aware of the linear sequence order.

To indicate the beginning or end of the sequence during sampling, it is necessary to define a start token and an end token, denoted as “CLS” and “SEP” respectively. During the training, the CLS token is concatenated to the amino acid sequence as the input, and the amino acid sequence concatenated with the SEP token is used as the label for model training.

The objective during the training phase is to minimize the negative log-likelihood, as shown in Eq. 2

$$\mathcal{L} = -\sum_{i=1}^n \log p(x_i | x_{<i}) \quad (2)$$

During the generation phase, peptides strings are generated using an autoregressive approach based on peptide fragments, which are then concatenated together as shown in Eq. 3

$$p(x) = \prod_{i=1}^n p(x_i | x_{<i}) \quad (3)$$

The generation process initiates with a start token, after which the model autoregressively generates amino acid tokens until reaching an end token.

### AMP-Prompt

To enable the model to generate peptide sequences with desired properties, we need to perform transfer learning on the pretrained peptide generation model AMP-GPT on a specified small dataset. Traditional language models tend to use a two-stage training approach, where they first pretrain on a large-scale corpus and then fine-tune on the downstream task, which can be affected by various factors such as data annotation quality and overfitting. In addition, for different downstream tasks, the entire model needs to be fine-tuned, which can consume a lot of computing resources.

In this task, we need to ensure that the generated peptides have multiple properties and high diversity as well. To address this issue, inspired by the work of Jing *et al.* (79), we use contrastive prompt tuning to perform transfer learning for the downstream task. As

shown in Fig. 1B, this prompt method belongs to the technique of soft prompt (38), where during training, we keep the AMP-GPT parameters frozen, initialize a prefix embedding layer for positive word labels, and initialize another prefix embedding layer for negative word labels. This design enables the model to acquire a better sense of distinction between positive and negative samples using prompts.

The design of the loss function is crucial in contrastive learning. The loss function for the contrastive prompt training consists of two parts: the language modeling training loss and the contrastive discriminative loss. The language modeling loss is modified from Eq. 2 by adding the prefix embedding as a condition. For each labeled sample  $(x, c)$  where  $x$  is the input sequence and  $c$  is the label, the language modeling loss can be defined as

$$\mathcal{L}_{\text{lm}} = - \sum_{i=1}^n \log p(x_i | x_{<i}, c) \quad (4)$$

The equation for the discriminative loss is as follows

$$\mathcal{L}_d = -\log \frac{p(x | c)}{p(x | c) + p(x | \bar{c})} \quad (5)$$

During training, the optimizer optimizes  $\mathcal{L}_d$  to improve the attribution  $p(c | y)$  by increasing  $p(x | c)$  and lowering  $p(x | \bar{c})$ .

The final loss function is shown as Eq. 6, and when  $\omega_1 = 1$ , there is no use of contrastive loss. At the same time, we used different sampling methods during generation: top- $k$  sampling and regular temperature sampling (80).

$$\mathcal{L}_{\text{contrast}} = \omega_1 \mathcal{L}_{\text{lm}} + \omega_2 \mathcal{L}_d \quad (6)$$

### AMP-Distillation

Using AMP-Prompt can improve the proportion of AMPs in the generated sequences, but our goal is to generate AMPs with increased activity as well as other desired properties. Therefore, our strategy involves optimizing the existing model through RL. However, directly FT RL on large models requires a lot of computation. To address this issue, we use knowledge distillation to distill the contrastive prompt-based AMP-Prompt with a smaller model.

Knowledge distillation is a model compression technique that aims at training a smaller model to mimic a larger pretrained model (or ensemble of models). This training setup is sometimes referred to as “teacher-student” with the large model as the teacher model and the small model as the student model. The method was first introduced by Buciluă *et al.* (81) in 2006.

The main idea is that certain knowledge regarding the dataset is transferred from a teacher model to a student model by minimizing the loss function. The goal of the student model is to learn the probability distribution predicted by the teacher model, which is the softmax layer’s output of the teacher model.

In this work, we used a RNN as the student model to learn AMP-Prompt, which we referred to as AMP-Distillation. To enable AMP-Distillation to learn more comprehensive information, different from the method proposed by Wang *et al.* (40), we trained it using soft-target distillation. Specifically, we used the probabilities output by the softmax layer of AMP-Prompt as the labels for training. The target function  $p_i$  can be defined as

$$p_i = \frac{\exp(z_i)}{\sum_j \exp(z_j)} \quad (7)$$

Through this approach, the AMP-Prompt model is transformed into an AMP-Distillation model that requires lower computational resources.

### Reinforcement learning

RL is widely used for FT pretrained neural networks. For example, RL is used to fine-tune RNNs for generating music with specific content (82). The success of this case demonstrates the feasibility of using RL for FT strategies in sequence models.

The goal of RL is to find an appropriate policy that maximizes the reward. In this work, we used the reward increment = nonnegative factor  $\times$  offset reinforcement  $\times$  characteristic eligibility (REINFORCE) (83) algorithm to fine-tune the AMP-Distillation. REINFORCE is a policy gradient-based RL algorithm that uses Monte Carlo to determine the optimal policy. As shown in Eq. 8, we use REINFORCE to optimize the pretrained model parameter  $\theta$  for the task of generating peptide sequences, so that the optimized model can generate peptides with desired properties and maximize the expected reward of each peptides sampling.

$$\theta' = \operatorname{argmax}_{\theta} \{ E_{\pi_0} [G(\tau)] \} \quad (8)$$

where  $\pi_0$  represents the policy with the model parameter  $\theta$ , and  $\tau$  represents the set of state-action pairs  $(s_t, a_t)$  in a trajectory from the initial state to the terminal state within  $T - 1$  steps, as shown in Eq. 9

$$\tau = (s_0, a_0, \dots, s_{T-1}, a_{T-1}) \quad (9)$$

The reward for each trajectory to the  $t$  step is  $r(s_t, a_t)$ . The sum of rewards from the  $t$  step to the final state is represented by Eq. 10

$$G(s_t, a_t) = \sum_{t=0}^{T-1} r(s_t, a_t) \quad (10)$$

According to the REINFORCE algorithm, the objective function can be derived as follows

$$J(\theta) = E_{\pi_0} [G(s_t, a_t)] = \left[ \sum_{t=0}^{T-1} \log \pi_0(s_t | a_t) G(s_t, a_t) \right] \quad (11)$$

In the task of generating peptide sequences,  $G(s_t, a_t)$  at each step in each trajectory cannot be calculated (the score of the complete peptide cannot be estimated based on the fragment of the peptide). Therefore, this task is a sparse reward problem in RL. To apply the REINFORCE algorithm to this task, the goal of the complete peptide is used as the score at each step, as shown in Eq. 12

$$G(s_t, a_t) = \sum_{t=0}^{T-1} r(s_t, a_t) = G(\tau) \quad (12)$$

The  $J(\theta)$  can be represented as

$$J(\theta) = G(\tau) \left[ \sum_{t=0}^{T-1} \log \pi_0(s_t | a_t) \right] \quad (13)$$

Combining with Eq. 11, we obtain

$$J(\theta) = G(\tau) \left[ \sum_{t=0}^{T-1} \log \pi_0(s_t | a_t) \right] = G(\tau) p(x | c) \quad (14)$$

Olivecrona *et al.* (84) proposed a target function that can improve the efficiency of RL FT compared to the target function in Eq. 14. The

specific steps are as follows: (i) copy the trained distillation model as an initialization agent model, sample peptide strings on the agent model, and save the likelihood value as  $\log P(S)_{\text{Agent}}$ ; (ii) input the generated peptide strings into the trained distillation model to obtain the likelihood value of the distillation model  $\log P(S)_{\text{Distilled}}$ ; (iii) multiply the reward  $S(S)$  calculated by the AMP-MIC by a coefficient  $\sigma$  and add  $\log P(S)_{\text{Distilled}}$  as the augmented likelihood  $\log P(A)_{\text{Agent}}$ .

$$\log P(A)_{\text{Aug}} = \log P(A)_{\text{distilled}} + \sigma S(A) \quad (15)$$

The loss function is defined as the augmented likelihood subtracted by the square of the likelihood of the agent model

$$\text{Loss} = [\log P(A)_{\text{Aug}} - \log P(A)_{\text{Agent}}]^2 \quad (16)$$

Setting  $G(\tau) = [\log P(A)_{\text{Aug}} - \log P(A)_{\text{Agent}}]^2 / \log P(A)_{\text{Aug}}$ , we can obtain Eq. 17 by combining with Eq. 14

$$J(\theta) = \text{Loss} = [\log P(A)_{\text{Aug}} - \log P(A)_{\text{Agent}}]^2 \quad (17)$$

Last, the loss function can be optimized through a gradient descent algorithm. In this study, we defined the reward as

$$G(\tau) = \omega_1 \text{CP} - \omega_2 \text{MIC} - \omega_3 \text{SL} - \omega_4 \text{MS} + \omega_5 \text{charge} \quad (18)$$

The variables involved in the equation have been previously explained in the “Designing high-activity peptides against Gram-negative bacteria” section.

### AMP-MIC

We fine-tuned the AMP-GPT on the MIC datasets of three bacterial species, namely *S. aureus*, *E. coli*, and *P. aeruginosa*, and compared it with GPT and LSTM prediction models.

### CT and FT models

To validate the effectiveness of prompt learning, we used the condition token (CT) and traditional full-model FT methods as the additional baselines in this study.

These models used the same backbone as AMP-GPT and use full model FT and CT for training and generation. As shown in fig. S5, the condition token method is retrained on labeled data, and a property label is added to the front of the model during training, which is used as the input during generation to autoregressively generate the entire peptide sequence. The traditional FT directly fine-tunes the AMP-GPT model using the real AMP dataset.

### Dataset

The dataset used in this study comprises of three distinct components. First, the training set of AMP-GPT was assembled from UniProt (85), whereby the peptides of length less than 32 were selected, followed by data cleaning processes to retain only the peptides with 20 amino acids. This process led to a final set of 630,683 peptides. The second component involved the use of label data to facilitate contrastive prompt learning, which was sourced from antimicrobial peptide database (APD3) (86), CAMP (87), database of antimicrobial activity and structure of peptides (DBAASP) (88), antimicrobial peptides database (DBAMP) (16), and data repository of antimicrobial peptides (DRAMP) (89). We retained monomers and natural AMP sequences, obtaining a total of 9896 AMPs. Subsequently, we filtered the DBAASP database for monomers and natural AMPs with target activities of  $\geq 100$ , resulting in 2303 non-AMPs. The third component was the dataset used to train

AMP-MIC, which integrated MIC values. In this part, we used the Gramapa (90) dataset, which featured over 51,345 laboratory peptide results. By processing the data using the code provided by Huang *et al.* (64), we obtained 4578 positive MIC data against *S. aureus*, 5102 positive MIC data against *E. coli*, 2853 positive MIC data against *P. aeruginosa*, and 8048 negative data. The data were then split into training, validation, and testing sets in a ratio of 75:15:10.

### Materials

The AMPs used in this study were custom-synthesized by Nanjing TGpeptide Biotechnology Co. Ltd., and their accurate molecular weights were determined by mass spectrometry. The purity of all peptides was determined by high-performance liquid chromatography (HPLC; column: kromasil C18, 5  $\mu\text{m}$ , 4.6 mm  $\times$  150 mm; wavelength: 214 nm), and all purity was greater than 95%. The abbreviations of AMPs and their corresponding sequences are shown in table S8.

Cyclophosphamide, norfloxacin, and Triton X-100 were purchased from Shanghai Macklin Biochemical Co. Ltd. COL was obtained from Bidepharm. Isoflurane was purchased from Shandong Ante Herding Technology Co. Ltd. All of the animal experiments performed in this research were approved by the Institutional Animal Care and Use Committee of the Guangzhou Institute of Biomedicine and Health (approval number: 2023079).

### Bacteria

The standard bacterial strains used in this work including *E. faecalis* ATCC 29212, *S. aureus* ATCC 29213, *K. pneumoniae* ATCC 700603, *A. baumannii* ATCC 19606, *P. aeruginosa* ATCC 27853, and *E. coli* ATCC 25922 were provided by microbiology laboratory of General Hospital of Southern Theatre Command. *P. acnes* ATCC 6919 and ATCC 11827 were purchased from Guangdong Microbial Culture Collection Center. PDR *K. pneumoniae* 418015, XDR *K. pneumoniae* 325016, MDR *K. pneumoniae* 327004, MDR *E. coli* 103231, MDR *P. aeruginosa* 304238, and MDR *A. baumannii* 316039 were isolated clinically from patients in the General Hospital of Southern Theatre Command, and their antimicrobial susceptibility testing results are displayed in table S6. All strains of ESKAPE pathogens were cultured aerobically at 37°C in cation-adjusted Mueller-Hinton broth (CAMHB) or Mueller-Hinton agar (MHA), while *P. acnes* were cultured anaerobically in Brain-Heart Infusion (BHI) broth or anaerobic blood agar.

### Mice

Male BALB/c mice (6 to 8 weeks, 18 to 22 g) were purchased from Guangdong Medical Laboratory Animal Center. All animal experiments were performed according to the “Principles of Laboratory Animal Care” (National Institutes of Health publication no. 86-23, revised 1985) and approved by the Institutional Animal Care and Use Committee.

### MIC determination

The MICs of AMPs against Gram-negative bacteria and aerobic Gram-positive bacteria were determined by broth microdilution method according to the guidelines of the Clinical and Laboratory Standards Institute. Briefly, AMPs were dissolved into sterile distilled water with an initial concentration of 5120  $\mu\text{g}/\text{ml}$  and stored at 4°C. In a sterile, plastic 96-well U-bottom plate, using a multichannel pipette, 100  $\mu\text{l}$  of CAMHB was added in wells of columns 2 to 12; subsequently, 200  $\mu\text{l}$  of the peptide solutions diluted to 1:10 with a final concentration of 512  $\mu\text{g}/\text{ml}$  was added to the column 1, and a

series of twofold dilutions was prepared by transferring 100  $\mu$ l to successive wells. The final test concentration of AMP was 256 to 0.125  $\mu$ g/ml, and three replicates of each peptide concentration were tested against each bacterial strain. A single colony of the bacterial strain was transferred to 4 ml of CAMHB and cultured at 37°C. After about 4 hours, the bacterial culture at the logarithmic phase was adjusted to 0.5 McFarland and diluted 1:100 with fresh CAMHB, and 100  $\mu$ l was added to 96-well plates containing AMPs to a final density of  $5 \times 10^5$  colony-forming units (CFU)/ml. Each test included a sterile blank control (CAMHB only), a growth (negative) control (CAMHB with bacterial inoculum but no peptide/antibiotic), and a positive control (COL against *E. coli* and *P. aeruginosa*, vancomycin against *E. faecalis* and *S. aureus*, and meropenem against *K. pneumoniae* and *A. baumannii*). After incubating at 37°C for 16 to 20 hours, the MIC results were taken as the minimal concentration of AMPs at which no visible bacterial growth was observed.

The MICs of AMPs against anaerobic Gram-positive bacteria were determined as described in (91). The *P. acnes* were inoculated into BHI medium and incubated in an anaerobic bag at 37°C to reach the logarithmic growth phase. The bacterial suspensions were prepared through centrifuged, resuspended in BHI medium three times, and then were diluted to a final concentration of  $1 \times 10^6$  CFU/ml. In a sterile, plastic 96-well U-bottom plate, using a multichannel pipette, 100  $\mu$ l of CAMHB was added in wells of columns 2 to 11; subsequently, 200  $\mu$ l of the peptide solutions diluted to 1:20 with a final concentration of 128  $\mu$ g/ml was added to the column 1, and a series of twofold dilutions was prepared by transferring 100  $\mu$ l to successive wells. The final test concentration of AMP was 64–0.0625  $\mu$ g/ml, and three replicates of each peptide concentration were tested against each bacterial strain. Then, 100- $\mu$ l aliquots of bacterial suspensions were added to each well. Each test included a sterile blank control (BHI only), a growth (negative) control (BHI with bacterial inoculum but no peptide/antibiotic), and a positive control (clindamycin). The MIC values were obtained as the lowest drug concentrations observed without any evidence of bacterial growth after 48-hour anaerobic culture.

### Time-kill assay

The *E. coli* culture, adjusted to 0.5 McFarland, was diluted 1:100 with fresh CAMHB medium and incubated at 37°C, 150 rpm for 3 to 4 hours to reach the logarithmic growth phase. The bacterial solution was then adjusted to 1 McFarland and diluted 1:100 in 10 ml of CAMHB medium containing the appropriate concentration of AMPs [KW13 (16  $\mu$ g/ml), AI18 (32  $\mu$ g/ml), and COL (2  $\mu$ g/ml)] and incubated at 37°C, 150 rpm. The time at which the bacterial solution was added was defined as 0 hours. At 0, 2, 4, 6, 18, and 24 hours, 200  $\mu$ l of bacteria solutions was taken out and was 10-fold serially diluted with fresh CAMHB medium in a sterile, 96-well U-bottom plate. Next, 10  $\mu$ l of each dilution was dropped onto MHA plates and incubated at 37°C for 18 to 24 hours to read the results. The assays were performed with three independent replicates. The lower limit of detection for the time-kill studies was 300 CFU/ml. These are based on dropping 10  $\mu$ l of bacterial solution and counting only dilutions of  $\geq 3$  and  $\leq 30$  CFUs.

### Hemolysis test

Fresh human red blood cells (RBCs) were washed three times with sterile PBS (800 g, centrifuged at 4°C for 5 min) and then added to

96-well U-bottom plates containing AMPs, making a concentration of 2% for RBCs and 100  $\mu$ g/ml for AMPs, with a final volume of 200  $\mu$ l. PBS-treated RBCs were used as negative control, and 0.5% Triton X-100-treated RBCs were used as positive control. After incubation at 37°C for 1 hour, the mixtures were centrifuged at 1200g for 15 min at 4°C. The supernatants were collected in new 96-well plates with a flat bottom, and the optical density at 570 nm ( $OD_{570}$ ) was measured. All experiments were performed with three independent replicates. The rate of hemolysis is calculated according to the following equation

$$\text{hemolysis (\%)} = \frac{OD_{570,\text{sample}} - OD_{570,\text{negative}}}{OD_{570,\text{positive}} - OD_{570,\text{negative}}} \quad (19)$$

### Resistance development in *E. coli*

To evaluate the resistance development during serial passage, *E. coli* ATCC 25922 cells were cultured to logarithmic growth phase, then adjusted to 0.5 McFarland, and diluted 1:100 into fresh CAMHB, and then 100  $\mu$ l of bacteria suspensions was added to 96-well plates containing twofold serial dilutions of varying concentrations of AMPs to a final volume of 200  $\mu$ l. MIC was obtained after incubating at 37°C without shaking for 24 hours. The cells that can grow in the wells with the highest concentration of AMPs were diluted 1:10000 into new 96-well plates containing fresh CAMHB and twofold serial diluted AMPs with varying concentrations again. The same procedure was performed every 24 hours and stopped after 30 days. Norfloxacin and COL were selected as control antibiotics. The change in an MIC value was recorded by taking the normalized value of MIC at generation X against the MIC value at generation 1.

### Plasma stability test

The sterile human blood was centrifuged at 3500 rpm for 10 min to obtain the supernatant as freshly prepared plasma. AMP was dissolved in water and freshly prepared plasma (1:1) to prepare a stock solution of 2500  $\mu$ g/ml.

Triplet tubes were gently shaken in an orbital shaker at 37°C (100 rpm), and 200  $\mu$ l of aliquots was collected at 0, 60, 120, and 240 min and added to 800  $\mu$ l of a mixture containing 10% methanol:10% water:80% acetonitrile and 1% acetic acid to stop further degradation of the peptides. The suspensions were centrifuged, and the supernatants were collected, filtered using a 0.45- $\mu$ m syringe filter, and analyzed by HPLC using the Agilent ZORBAX C18 reverse-phase analytical column (5  $\mu$ m, 4.6 mm by 250 mm). The mobile phases were acetonitrile [containing 0.1% trifluoroacetic acid (TFA)] and deionized water (containing 0.1% TFA), and the elution system used was from 10 to 99% acetonitrile, the analytic time was 33 min, the flow rate was 1 ml/min, and absorbance was measured at a wavelength of 214 nm.

### Membrane disruption detected by TEM

A single colony of *E. coli* ATCC 25922 was cultured in 60 ml of CAMHB medium overnight to the logarithmic growth phase at 37°C, and then bacteria cells were collected by centrifugation at 4000 rpm for 5 min at room temperature and resuspended with PBS (pH 7.0) to an  $OD_{600}$  of 1.0. Ten milliliters of the bacterial suspensions was treated with AMP at final concentrations of 1× MIC and 10× MIC at 37°C for 5 hours, and untreated cells were used as control.

Samples were washed with PBS three times and prefixed with 1 ml of 3% glutaraldehyde (v/v) in PBS at 4°C for 3 hours. After washing with PBS two times in 10 min, samples were postfixed with 1% osmium acid for 2 hours at room temperature and then washed with PBS two times in 5 min. Thereafter, the specimens were subsequently dehydrated in ethanol series (10 min each: 50 and 70%) and acetone series (10 min  $\times$  2: 80, 90, and 100%). Subsequently, the specimens were displaced in a mixture of acetone and epoxy resin Epon812 (1:1 for 40 min), infiltrated in epoxy resin Epon812 overnight at 37°C, and lastly embedded in epoxy resin Epon812 at 60°C for 48 hours in a cylindrical mold. Ultrathin sections of 40-nm thickness using Leica ultramicrotome were then carefully transferred to a copper grid and dried overnight. These copper grids were poststained with saturated uranyl acetate (prepared with 70% ethanol) for 3 min and lead citrate for 3 min and dried completely. The images were taken with a TEM (HITACHI H-7650).

### Neutropenic mouse pneumonia model

Twenty-four healthy male BALB/c mice (6 to 8 weeks,  $20 \pm 2$  g) were injected intraperitoneally with cyclophosphamide (dissolved in sterile PBS) 4 days and 1 day before bacterial infection, at concentrations of 150 and 100 mg/kg, respectively, to induce neutropenia. On the day of infection, mice were anesthetized with isoflurane and then suspended by their upper front teeth from a nylon string on an angled plexiglass platform. Forty microliters of log-phase grown *K. pneumoniae* 325016 ( $1 \times 10^6$  CFU/ml in PBS) loaded in a pipette was instilled into the lungs by compressing air. Mice were held upright for 30 s to allow bacteria inoculum to be inhaled into the lungs. Subsequently, the mice were randomly divided into four groups of six mice each. The mice were injected intraperitoneally with KW13 (10 mg/kg), AI18, indolicidin, or an equivalent amount of PBS at 2 and 12 hours postinfection, respectively. All mice were euthanized at 24 hours after infection, and the left lung tissues were collected under aseptic conditions, weighed, and homogenized with 1 ml of sterile PBS. The homogenate was diluted with sterile PBS in a 10-fold gradient and plated onto MHA plates and incubated at 37°C for 18 to 24 hours, then colonies were counted, and the bacterial load of lung tissue was calculated. Histological analyses were conducted after the right lung tissues were collected and fixed by 4% formalin overnight and embedded in paraffin for hematoxylin and eosin (H&E) staining.

### Statistical analysis

Statistical analysis was conducted using one-way analysis of variance. The data were analyzed using statistical software of GraphPad Prism version 8.0 (Chicago, IL, USA). Quantitative data were expressed as mean  $\pm$  SD, and  $P < 0.05$  was considered statistically significant.

### Supplementary Materials

#### This PDF file includes:

Supplementary Text

Figs. S1 to S6

Tables S1 to S8

### REFERENCES AND NOTES

- Antimicrobial Resistance Collaborators, Global burden of bacterial antimicrobial resistance in 2019: A systematic analysis. *Lancet* **399**, 629–655 (2022).
- J. O'Neill, *Tackling drug-resistant infections globally: Final report and recommendations*. Review on Antimicrobial Resistance. (2016).
- K. Lewis, Platforms for antibiotic discovery. *Nat. Rev. Drug Discov.* **12**, 371–387 (2013).
- Z. Lyu, P. Yang, J. Lei, J. Zhao, Biological function of antimicrobial peptides on suppressing pathogens and improving host immunity. *Antibiotics* **12**, 1037 (2023).
- D. Mathur, S. Singh, A. Mehta, P. Agrawal, G. P. S. Raghava, In silico approaches for predicting the half-life of natural and modified peptides in blood. *PLOS ONE* **13**, e0196829 (2018).
- B. Gomes, M. T. Augusto, M. R. Felício, A. Hollmann, O. L. Franco, S. Gonçalves, N. C. Santos, Designing improved active peptides for therapeutic approaches against infectious diseases. *Biotechnol. Adv.* **36**, 415–429 (2018).
- J. P. Bradshaw, Cationic antimicrobial peptides. *BioDrugs* **17**, 233–240 (2003).
- A. K. Marr, W. J. Gooderham, R. E. W. Hancock, Antibacterial peptides for therapeutic use: Obstacles and realistic outlook. *Curr. Opin. Pharmacol.* **6**, 468–472 (2006).
- M. H. Cardoso, R. Q. Orozco, S. B. Rezende, G. Rodrigues, K. G. N. Oshiro, E. S. Cândido, O. L. Franco, Computer-aided design of antimicrobial peptides: Are we generating effective drug candidates? *Front. Microbiol.* **10**, 3097 (2020).
- X. Xiao, P. Wang, W.-Z. Lin, J.-H. Jia, K.-C. Chou, iAMP-2L: A two-level multi-label classifier for identifying antimicrobial peptides and their functional types. *Anal. Biochem.* **436**, 168–177 (2013).
- L. C. H. W. Fingerhut, D. J. Miller, J. M. Strugnell, N. L. Daly, I. R. Cooke, amipr: An R package for fast genome-wide prediction of antimicrobial peptides. *Bioinformatics* **36**, 5262–5263 (2021).
- M. N. Gabere, W. S. Noble, Empirical comparison of web-based antimicrobial peptide prediction tools. *Bioinformatics* **33**, 1921–1929 (2017).
- C. Li, D. Sutherland, S. A. Hammond, C. Yang, F. Taho, L. Bergman, S. Houston, R. L. Warren, T. Wong, L. M. N. Hoang, C. E. Cameron, C. C. Helbing, I. Birol, AMPify: Attentive deep learning model for discovery of novel antimicrobial peptides effective against WHO priority pathogens. *BMC Genomics* **23**, 77 (2022).
- S. Gull, N. Shamim, F. Mirhas, AMAP: Hierarchical multi-label prediction of biologically active and antimicrobial peptides. *Comput. Biol. Med.* **107**, 172–181 (2019).
- M. Burdakiewicz, K. Sidorczuk, D. Rafacz, P. Pietluch, J. Chilimoniuk, S. Rödiger, P. Gagat, Proteomic screening for prediction and design of antimicrobial peptides with AmpGram. *Int. J. Mol. Sci.* **21**, 4310 (2020).
- J.-H. Jhong, Y.-H. Chi, W.-C. Li, T.-H. Lin, K.-Y. Huang, T.-Y. Lee, dbAMP: An integrated resource for exploring antimicrobial peptides with functional activities and physicochemical properties on transcriptome and proteome data. *Nucleic Acids Res.* **47**, D285–D297 (2019).
- W. F. Porto, Á. S. Pires, O. L. Franco, CS-AMPPred: An updated SVM model for antimicrobial activity prediction in cysteine-stabilized peptides. *PLOS ONE* **7**, e51444 (2012).
- P. Wang, L. Hu, G. Liu, N. Jiang, X. Chen, J. Xu, W. Zheng, L. Li, M. Tan, Z. Chen, H. Song, Y.-D. Cai, K.-C. Chou, Prediction of antimicrobial peptides based on sequence alignment and feature selection methods. *PLOS ONE* **6**, e18476 (2011).
- C. M. Van Oort, J. B. Ferrell, J. M. Remington, S. Wshah, J. Li, AMPGAN v2: Machine learning-guided design of antimicrobial peptides. *J. Chem. Inf. Model.* **61**, 2198–2207 (2021).
- K. Browne, S. Chakraborty, R. Chen, M. D. Willcox, D. S. Black, W. R. Walsh, N. Kumar, A new era of antibiotics: The clinical potential of antimicrobial peptides. *Int. J. Mol. Sci.* **21**, 7047 (2020).
- F. Wan, D. Kontogiorgos-Heintz, C. de la Fuente-Nunez, Deep generative models for peptide design. *Digit. Discov.* **1**, 195–208 (2022).
- F. Wan, C. de la Fuente-Nunez, Mining for antimicrobial peptides in sequence space. *Nat. Biomed. Eng.* **7**, 707–708 (2023).
- A. T. Müller, J. A. His, G. Schneider, Recurrent neural network model for constructive peptide design. *J. Chem. Inf. Model.* **58**, 472–479 (2018).
- D. Nagarajan, T. Nagarajan, N. Roy, O. Kulkarni, S. Ravichandran, M. Mishra, D. Chakravortty, N. Chandra, Computational antimicrobial peptide design and evaluation against multidrug-resistant clinical isolates of bacteria. *J. Biol. Chem.* **293**, 3492–3509 (2018).
- C. Wang, S. Garlick, M. Zloh, Deep learning for novel antimicrobial peptide design. *Biomolecules* **11**, 471 (2021).
- A. Rossetto, W. Zhou, paper presented at the Proceedings of the 11th ACM International Conference on Bioinformatics, Computational Biology and Health Informatics, Virtual Event, USA, 2020.
- J. B. Ferrell, J. M. Remington, C. M. V. Oort, M. Sharafi, R. Aboushousha, Y. Janssen-Heininger, S. T. Schneebeli, M. J. Wargo, S. Wshah, J. Li, A generative approach toward precision antimicrobial peptide design. bioRxiv 324087 [Preprint] (2020). <https://doi.org/10.1101/2020.10.02.324087>.
- A. Tucs, D. P. Tran, A. Yumoto, Y. Ito, T. Uzawa, K. Tsuda, Generating ampicillin-level antimicrobial peptides with activity-aware generative adversarial networks. *ACS Omega* **5**, 22847–22851 (2020).
- S. Surana, P. Arora, D. Singh, D. Sahasrabuddhe, J. Valadi, PandoraGAN: Generating antiviral peptides using generative adversarial network. *SN Comput. Sci.* **4**, 607 (2023).
- P. Das, K. Wadhawan, O. Chang, T. Sercu, C. Dos Santos, M. Riemer, V. Chenthamarakshan, I. Padhi, A. Mojsilovic, PepCVAE: Semi-supervised targeted design of antimicrobial peptide sequences. arXiv:1810.07743 [q-bio.QM] (2018).

31. S. N. Dean, S. A. Walper, Variational autoencoder for generation of antimicrobial peptides. *ACS Omega* **5**, 20746–20754 (2020).
32. P. Das, T. Sercu, K. Wadhawan, I. Padhi, S. Gehrmann, F. Cipcigan, V. Chenthamarakshan, H. Strobel, C. dos Santos, P.-Y. Chen, Y. Yang, J. P. K. Tan, J. Hedrick, J. Crain, A. Mojsilovic, Accelerated antimicrobial discovery via deep generative models and molecular dynamics simulations. *Nat. Biomed. Eng.* **5**, 613–623 (2021).
33. Q. Chen, C. Yang, Y. Xie, Y. Wang, X. Li, K. Wang, J. Huang, W. Yan, GM-Pep: A high efficiency strategy to de novo design functional peptide sequences. *J. Chem. Inf. Model.* **62**, 2617–2629 (2022).
34. M. Mirza, S. Osindero, Conditional generative adversarial nets. arXiv.1411.1784 [cs.LG] (2014).
35. K. Sohn, X. Yan, H. Lee, paper presented at the Proceedings of the 28th International Conference on Neural Information Processing Systems - Volume 2, Montreal, Canada. (2015).
36. F. Grisoni, C. S. Neuhaus, G. Gabernet, A. T. Müller, J. A. Hiss, G. Schneider, Designing anticancer peptides by constructive machine learning. *ChemMedChem* **13**, 1300–1302 (2018).
37. A. Capecci, X. Cai, H. Personne, T. Köhler, C. van Delden, J.-L. Reymond, Machine learning designs non-hemolytic antimicrobial peptides. *Chem. Sci.* **12**, 9221–9232 (2021).
38. B. Lester, R. Al-Rfou, N. Constant, Online and Punta Cana, Dominican Republic, November 2021.
39. T. Gao, A. Fisch, D. Chen. (Association for computational linguistics, online, 2021), pp. 3816–3830.
40. J. Wang, C.-Y. Hsieh, M. Wang, X. Wang, Z. Wu, D. Jiang, B. Liao, X. Zhang, B. Yang, Q. He, D. Cao, X. Chen, T. Hou, Multi-constraint molecular generation based on conditional transformer, knowledge distillation and reinforcement learning. *Nat. Mach. Intell.* **3**, 914–922 (2021).
41. V. Chenthamarakshan, S. C. Hoffman, C. D. Owen, P. Lukacik, C. Strain-Damerell, D. Fearon, T. R. Malla, A. Tumber, C. J. Schofield, H. M. E. Duyvesteyn, W. Dejnirattisai, L. Carrique, T. S. Walter, G. R. Scream, T. Matviuk, A. Mojsilovic, J. Crain, M. A. Walsh, D. I. Stuart, P. Das, Accelerating drug target inhibitor discovery with a deep generative foundation model. *Sci. Adv.* **9**, eadg7865 (2023).
42. J. Wang, C. Wang, F. Luo, C. Tan, M. Qiu, F. Yang, Q. Shi, S. Huang, M. Gao, Abu Dhabi, United Arab Emirates, December 2022.
43. T. Xiao, Y. Dong, B. Dong, Output Layer Go First: Better Fine-tuning by Bridging the Gap with Pre-training, in *International Conference on Natural Language Processing* (ICNLP, 2021), pp. 145–149.
44. A. Radford, K. Narasimhan, T. Salimans, I. Sutskever, Improving language understanding by generative pre-training. (2018).
45. S. Dathathri, A. Madotto, J. Lan, J. Hung, E. Frank, P. Molino, J. Yosinski, R. Liu, Plug and play language models: A simple approach to controlled text generation. arXiv.1912.02164 [cs.CL] (2019).
46. UniProt Consortium, UniProt: The universal protein knowledgebase in 2021. *Nucleic Acids Res.* **49**, D480–D489 (2020).
47. J. Devlin, M.-W. Chang, K. Lee, K. Toutanova, BERT: Pre-training of deep bidirectional transformers for language understanding. arXiv.1810.04805 [cs.CL] (2018).
48. T. B. Brown, B. Mann, N. Ryder, M. Subbiah, J. Kaplan, P. Dhariwal, A. Neelakantan, P. Shyam, G. Sastry, A. Askell, S. Agarwal, A. Herbert-Voss, G. Krueger, T. Henighan, R. Child, A. Ramesh, D. M. Ziegler, J. Wu, C. Winter, C. Hesse, M. Chen, E. Sigler, M. Litwin, S. Gray, B. Chess, J. Clark, C. Berner, S. McCandlish, A. Radford, I. Sutskever, D. Amodei, Language models are few-shot learners. arXiv.2005.14165 [cs.CL] (2020).
49. M. E. Peters, M. Neumann, M. Iyyer, M. Gardner, C. Clark, K. Lee, L. Zettlemoyer, Deep Contextualized Word Representations, In Association for Computational Linguistics (ACL, 2018), pp. 2227–2237.
50. B. McCann, J. Bradbury, C. Xiong, R. Socher, paper presented at the Proceedings of the 31st International Conference on Neural Information Processing Systems (Long Beach, California, USA, 2017).
51. A. Madani, B. Krause, E. R. Greene, S. Subramanian, B. P. Mohr, J. M. Holton, J. L. Olmos, C. Xiong, Z. Z. Sun, R. Socher, J. S. Fraser, N. Naik, Large language models generate functional protein sequences across diverse families. *Nat. Biotechnol.* **41**, 1099–1106 (2023).
52. N. Ferruz, S. Schmidt, B. Höcker, ProtGPT2 is a deep unsupervised language model for protein design. *Nat. Commun.* **13**, 4348 (2022).
53. Z. Lin, H. Akin, R. Rao, B. Hie, Z. Zhu, W. Lu, N. Smetanin, R. Verkuil, O. Kabeli, Y. Shmueli, A. dos Santos Costa, M. Fazel-Zarandi, T. Sercu, S. Candido, A. Rives, Evolutionary-scale prediction of atomic-level protein structure with a language model. *Science* **379**, 1123–1130 (2023).
54. J. Ficler, Y. Goldberg, Controlling Linguistic Style Aspects in Neural Language Generation, in Association for Computational Linguistics (ACL, 2017), pp. 94–104.
55. A. Fan, M. Lewis, Y. Dauphin. (Association for Computational Linguistics, Melbourne, Australia, 2018), pp. 889–898.
56. A. T. Müller, G. Gabernet, J. A. Hiss, G. Schneider, modIAMP: Python for antimicrobial peptides. *Bioinformatics* **33**, 2753–2755 (2017).
57. D. Eisenberg, R. M. Weiss, T. C. Terwilliger, The helical hydrophobic moment: A measure of the amphiphilicity of a helix. *Nature* **299**, 371–374 (1982).
58. U. Gawde, S. Chakraborty, F. H. Waghu, R. S. Barai, A. Khanderkar, R. Indraguru, T. Shirsat, S. Idicula-Thomas, CAMPR4: A database of natural and synthetic antimicrobial peptides. *Nucleic Acids Res.* **51**, D377–D383 (2023).
59. D. Veltri, U. Kamath, A. Shehu, Deep learning improves antimicrobial peptide recognition. *Bioinformatics* **34**, 2740–2747 (2018).
60. C. D. Santos-Júnior, S. Pan, X. M. Zhao, L. P. Coelho, Macrel: Antimicrobial peptide screening in genomes and metagenomes. *PeerJ* **8**, e10555 (2020).
61. A. Pandi, D. Adam, A. Zare, V. T. Trinh, S. L. Schaefer, M. Burt, B. Klabunde, E. Bobkova, M. Kushwaha, Y. Foroughijabbari, P. Braun, C. Spahn, C. Preußen, E. Pogge von Strandmann, H. B. Bode, H. von Buttlar, W. Bertram, A. L. Jung, F. Abendroth, B. Schmeck, G. Hummer, O. Vázquez, T. J. Erb, Cell-free biosynthesis combined with deep learning accelerates de novo-development of antimicrobial peptides. *Nat. Commun.* **14**, 7197 (2023).
62. P. J. A. Cock, T. Antao, J. T. Chang, B. A. Chapman, C. J. Cox, A. Dalke, I. Friedberg, T. Hamelryck, F. Kauff, B. Wilczynski, M. J. L. de Hoon, Biopython: Freely available Python tools for computational molecular biology and bioinformatics. *Bioinformatics* **25**, 1422–1423 (2009).
63. K. Sidorczuk, P. Gagat, F. Pietluch, J. Kala, D. Rafacz, L. Bałka, J. Słowiak, R. Kolenda, S. Rödiger, L. C. H. W. Fingerhut, I. R. Cooke, P. Mackiewicz, M. Burdukiewicz, Benchmarks in antimicrobial peptide prediction are biased due to the selection of negative data. *Brief. Bioinform.* **23**, bbbac343 (2022).
64. J. Huang, Y. Xu, Y. Xue, Y. Huang, X. Li, X. Chen, Y. Xu, D. Zhang, P. Zhang, J. Zhao, J. Ji, Identification of potent antimicrobial peptides via a machine-learning pipeline that mines the entire space of peptide sequences. *Nat. Biomed. Eng.* **7**, 797–810 (2023).
65. K. Chaudhary, R. Kumar, S. Singh, A. Tukenait, A. Gautam, D. Mathur, P. Anand, G. C. Varshney, G. P. S. Raghava, A web server and mobile app for computing hemolytic potency of peptides. *Sci. Rep.* **6**, 22843 (2016).
66. S. Gupta, P. Kapoor, K. Chaudhary, A. Gautam, R. Kumar, G. P. S. Raghava, “Peptide toxicity prediction” in *Computational Peptidology*, P. Zhou, J. Huang, Eds. (Springer New York, 2015), pp. 143–157.
67. S. Gupta, P. Kapoor, K. Chaudhary, A. Gautam, R. Kumar, G. P. S. Raghava, In silico approach for predicting toxicity of peptides and proteins. *PLOS ONE* **8**, e73957 (2013).
68. Lens. Patseqfinder. Retrieved May 12, from <https://lens.org/lens/bio/patseqfinder> (2023).
69. N. Mookherjee, M. A. Anderson, H. P. Haagsman, D. J. Davidson, Antimicrobial host defence peptides: Functions and clinical potential. *Nat. Rev. Drug Discov.* **19**, 311–332 (2020).
70. A. Mazurkiewicz-Pisarek, J. Baran, T. Ciach, Antimicrobial peptides: Challenging journey to the pharmaceutical, biomedical, and cosmeceutical use. *Int. J. Mol. Sci.* **24**, 9031 (2023).
71. Y. Shi, J. Hu, P. Liu, T. Wang, H. Wang, Y. Liu, Q. Cao, X. Zuo, Ceftazidime–avibactam-based versus tigecycline-based regimen for the treatment of carbapenem-resistant klebsiella pneumoniae-induced pneumonia in critically ill patients. *Infect. Dis. Ther.* **10**, 2721–2734 (2021).
72. S. Bera, A. Ghosh, S. Sharma, T. Debnath, B. Giri, A. Bhunia, Probing the role of Proline in the antimicrobial activity and lipopolysaccharide binding of indolicidin. *J. Colloid Interface Sci.* **452**, 148–159 (2015).
73. J. Batista Araujo, G. Sastre de Souza, E. N. Lorenzon, Indolicidin revisited: Biological activity, potential applications and perspectives of an antimicrobial peptide not yet fully explored. *World J. Microbiol. Biotechnol.* **38**, 39 (2022).
74. GBD 2015 Disease and Injury Incidence and Prevalence Collaborators, Global, regional, and national incidence, prevalence, and years lived with disability for 310 diseases and injuries, 1990–2015: A systematic analysis for the Global Burden of Disease Study 2015. *Lancet* **388**, 1545–1602 (2016).
75. D. E. Castillo, S. Nanda, J. E. Keri, Propionibacterium (*Cutibacterium*) acnes bacteriophage therapy in acne: Current evidence and future perspectives. *Dermatol. Ther.* **9**, 19–31 (2019).
76. P. Sermwan, R. Sriharat, S. Saithong, M. Laowansiri, N. Amornruk, D. Chiewchengchol, N. Noppakun, P. Asawanonda, T. Chatsuwan, C. Kumtorornrut, A cross-sectional study examining the prevalence of antibiotic-resistant *Cutibacterium* acnes isolated from patients with acne in Bangkok, Thailand. *J. Dermatol.* **50**, 1008–1013 (2023).
77. C. Dessinioti, A. Katsambas, Antibiotics and antimicrobial resistance in acne: Epidemiological trends and clinical practice considerations. *Yale J. Biol. Med.* **95**, 429–443 (2022).
78. A. Vaswani, N. Shazeer, N. Parmar, J. Uszkoreit, L. Jones, A. N. Gomez, Ł. Kaiser, I. Polosukhin, paper presented at the Advances in Neural Information Processing Systems, 2017.
79. J. Qian, L. Dong, Y. Shen, F. Wei, W. Chen, Controllable Natural Language Generation with Contrastive Prefixes, in Association for Computational Linguistics (ACL, 2022), pp. 2912–2924.
80. I. Sutskever, J. Martens, G. Hinton, paper presented at the Proceedings of the 28th International Conference on International Conference on Machine Learning, Bellevue, Washington, USA, 2011.
81. C. Buciuă, R. Caruana, A. Niculescu-Mizil, paper presented at the Proceedings of the 12th ACM SIGKDD International Conference on Knowledge Discovery and Data Mining, 2006.
82. N. Jaques, S. Gu, R. Turner, D. Eck, Tuning recurrent neural networks with reinforcement learning. arXiv:1611.02796v02791 (2016).
83. R. J. Williams, Simple statistical gradient-following algorithms for connectionist reinforcement learning. *Mach. Learn.* **8**, 229–256 (1992).

84. M. Olivecrona, T. Blaschke, O. Engkvist, H. Chen, Molecular de-novo design through deep reinforcement learning. *J. Cheminformatics* **9**, 48 (2017).
85. The UniProt Consortium, UniProt: The universal protein knowledgebase. *Nucleic Acids Res.* **45**, D158–D169 (2017).
86. G. Wang, X. Li, Z. Wang, APD3: The antimicrobial peptide database as a tool for research and education. *Nucleic Acids Res.* **44**, D1087–D1093 (2016).
87. S. Thomas, S. Karnik, R. S. Barai, V. K. Jayaraman, S. Idicula-Thomas, CAMP: A useful resource for research on antimicrobial peptides. *Nucleic Acids Res.* **38**, D774–D780 (2010).
88. M. Pirtskhalava, A. A. Armstrong, M. Grigolava, M. Chubinidze, E. Alimbarashvili, B. Vishnepolsky, A. Gabrielian, A. Rosenthal, D. E. Hurt, M. Tartakovsky, DBAASP v3: Database of antimicrobial/cytotoxic activity and structure of peptides as a resource for development of new therapeutics. *Nucleic Acids Res.* **49**, D288–D297 (2021).
89. X. Kang, F. Dong, C. Shi, S. Liu, J. Sun, J. Chen, H. Li, H. Xu, X. Lao, H. Zheng, DRAMP 2.0, an updated data repository of antimicrobial peptides. *Sci. Data* **6**, 148 (2019).
90. W. Jacob, W. Zack, Deep learning regression model for antimicrobial peptide design. bioRxiv 692681 [Preprint] (2019). <https://doi.org/10.1101/692681>.
91. G. Yang, J. Wang, S. Lu, Z. Chen, S. Fan, D. Chen, H. Xue, W. Shi, J. He, Short lipopeptides specifically inhibit the growth of Propionibacterium acnes with a dual antibacterial and anti-inflammatory action. *Br. J. Pharmacol.* **176**, 2321–2335 (2019).
- (J.W.) and 2023TQ0285 (J.W.); Postdoctoral Fellowship Program of CPSF GZB20230657 (J.W.); Natural Science Foundation of Guangdong Province Youth Enhancement Project 2023A1515030153 (Z.J.); Key Basic Project of General Hospital of Southern Theatre Command 2022NZA001 (Z.J.); and Joint Fund of Guangzhou Basic Research Program 2024A03J0644 (Z.J.). **Author contributions:** Project administration: C.-Y.H., Z.J., and T.H. Conceptualization: J.W., Y.K., Xingcai Zhang, C.-Y.H., Z.J., and T.H. Data curation: J.W., M.W., G.Y., and Z.J. Formal analysis: J.W., J.F., G.Y., M.W., Z.W., J.Y., LW., Y.W., J.G., T.W., and Z.J. Investigation: J.W., J.F., J.Y., LW., Y.W., Z.J., and T.H. Methodology: J.W., J.F., Y.K., M.W., Z.J., and T.H. Resources: J.W., J.F., Y.K., PP., J.Y., LW., Y.W., C.-Y.H., Z.J., and T.H. Funding acquisition: J.W., Y.K., PP., Z.J., and T.H. Visualization: J.W., J.F., Y.K., Xingcai Zhang, and Z.J. Software: J.W. Supervision: Y.K., PP., H.S., Y.D., C.-Y.H., Z.J., and T.H. Validation: J.W., J.F., LW., Y.W., Xingcai Zhang, and Z.J. Writing—original draft: J.W., J.F., Y.K., M.W., Z.J., and T.H. Writing—review and editing: J.W., J.F., Y.K., PP., M.W., Xujun Zhang, Xingcai Zhang, C.-Y.H., Z.J., and T.H. **Competing interests:** The authors declare that they have no competing interests. **Data and materials availability:** All data needed to evaluate the conclusions in the paper are present in the paper and/or the Supplementary Materials. The dataset used in this investigation consists of three components. First, the UniProt (85) database was used to retrieve peptides with a length less than 32. The second component involved label data obtained from multiple sources, namely APD3 (86), CAMP (87), DBAASP (88), DBAMP (16), and DRAMP (89). The third component encompasses the MIC data, sourced from the Gramapa (90) dataset. The code used in the study can be found at <https://github.com/jkwang93/AMP-Designer> or at <https://doi.org/10.5281/zenodo.13999503>.

**Acknowledgments**

**Funding:** This work was financially supported by National Key Research and Development Program of China 2024YFA1307501 (T.H.) and 2022YFF1203000 (PP.); National Natural Science Foundation of China 82204279 (PP.), 82373791 (Y.K.), and 22303083 (J.W.); Fundamental Research Funds for the Central Universities 226-2022-00220 (P.P.); China Postdoctoral Science Foundation 2023M733128

Submitted 2 September 2024

Accepted 29 January 2025

Published 5 March 2025

10.1126/sciadv.ads8932